Title

Protection against corneal hyperosmolarity with soft-contact-lens wear

Authors

Kim, Young Hyun
Nguyen, Thien
Lin, Meng C
et al.

Publication Date

2022-03-01

DOI

10.1016/j.preteyeres.2021.101012

Peer reviewed

Progress in Retinal and Eye Research 87 (2022) 101012

Contents lists available at ScienceDirect

Progress in Retinal and Eye Research

journal homepage: www.elsevier.com/locate/preteyeres

Invited Review Article

Protection against corneal hyperosmolarity with soft-contact-lens wear

Young Hyun Kim [a,b,c], Thien Nguyen [b], Meng C. Lin [a,c], Cheng-Chun Peng [d], Clayton J. Radke [a,b,*]

[a] Vision Science Group, University of California, Berkeley, CA, 94720, United States
[b] Chemical and Biomolecular Engineering Department, University of California, Berkeley, CA, 94720, United States
[c] Clinical Research Center, School of Optometry, University of California, Berkeley, CA, 94720, United States
[d] CooperVision, Inc, Pleasanton, CA, 94588, United States

ARTICLE INFO

Keywords:
Tear osmolarity
Post-lens tear-film osmolarity
Contact-lens wear discomfort
Soft contact lens
Hyperosmolarity
Lens-salt diffusivity
Dry eye

ABSTRACT

Hyperosmotic tear stimulates human corneal nerve endings, activates ocular immune response, and elicits dry-eye symptoms. A soft contact lens (SCL) covers the cornea preventing it from experiencing direct tear evaporation and the resulting blink-periodic salinity increases. For the cornea to experience hyperosmolarity due to tear evaporation, salt must transport across the SCL to the post-lens tear film (PoLTF) bathing the cornea. Consequently, limited salt transport across a SCL potentially protects the ocular surface from hyperosmotic tear. In addition, despite lens-wear discomfort sharing common sensations to dry eye, no correlation is available between measured tear hyperosmolarity and SCL-wear discomfort. Lack of documentation is likely because clinical measurements of tear osmolarity during lens wear do not interrogate the tear osmolarity of the PoLTF that actually overlays the cornea. Rather, tear osmolarity is clinically measured in the tear meniscus. For the first time, we mathematically quantify tear osmolarity in the PoLTF and show that it differs significantly from the clinically measured tear-meniscus osmolarity. We show further that aqueous-deficient dry eye and evaporative dry eye both exacerbate the hyperosmolarity of the PoLTF. Nevertheless, depending on lens salt-transport properties (i.e., diffusivity, partition coefficient, and thickness), a SCL can indeed protect against corneal hyperosmolarity by reducing PoLTF salinity to below that of the ocular surface during no-lens wear. Importantly, PoLTF osmolarity for dry-eye patients can be reduced to that of normal eyes with no-lens wear provided that the lens exhibits a low lens-salt diffusivity. Infrequent blinking increases PoLTF osmolarity consistent with lens-wear discomfort. Judicious design of SCL material salt-transport properties can ameliorate corneal hyperosmolarity. Our results confirm the importance of PoLTF osmolarity during SCL wear and indicate a possible relation between PoLTF osmolarity and contact-lens discomfort.

1. Introduction

Numerous clinical studies of tear-meniscus osmolarity demonstrate that dry-eye patients exhibit higher tear osmolarity than those with normal healthy eyes (Farris, 1986; Farris et al, 1981, 1983; Gilbard, 1994; Gilbard et al., 1978; Mathers et al., 1996; Mishima et al., 1971; Ogasawara et al., 1996). Tomlinson et al. (2006) compiled tear-meniscus osmolarities from studies conducted between 1978 and 2004 and determined that the mean values for normal and dry eyes are 302.2 and 326.9 milliosmolar (mOsM), respectively. Since then, a prospective, multicenter study by Lemp et al. (2011) showed that tear-meniscus osmolarity has the highest sensitivity and specificity to detect dry eye compared to tear-film break-up time (TBUT), corneal staining, conjunctival staining, Schirmer tear test, and meibomian-gland grading. In contrast, some studies found no significant correlation between osmolarity and dry-eye symptoms (Amparo et al., 2014; Yeh et al., 2015).

Tear osmolarity is determined by the dissolved solute concentrations which, in turn, depend on tear production, evaporation, and drainage (Baudouin et al., 2013; Tomlinson and Khanal, 2005). Clinically measured tear osmolarity (Amparo et al., 2014; Farris, 1986; Farris et al, 1981, 1983; Gilbard, 1994; Gilbard et al., 1978; Mathers et al., 1996; Mishima et al., 1971; Ogasawara et al., 1996; Tomlinson et al., 2006; Yeh et al., 2015) usually corresponds to that in the lower tear meniscus, which is significantly lower than that of the pre-corneal tear film (PrCTF) (Bron et al., 2002; Cerretani and Radke, 2014; Gaffney et al.,

* Corresponding author. Department of Chemical and Biomolecular Engineering, University of California, 101E Gilman Hall, Berkeley, CA, 94720.
E-mail address: radke@berkeley.edu (C.J. Radke).

https://doi.org/10.1016/j.preteyeres.2021.101012
Received 16 July 2021; Received in revised form 18 September 2021; Accepted 21 September 2021
Available online 29 September 2021

2010). The no-lens modeling analysis of Cerretani and Radke (2014) in Fig. 1 contrasts the periodic excursions of osmolarity in the PrCTF relative to the menisci for both normal and dry eyes. This figure demonstrates that dry-eye menisci and PrCTF osmolarities can differ by more than 10 mOsM. Higher osmolarity of the PrCTF than that in the menisci is due to the larger surface area for evaporation and the smaller tear volume of the PrCTF, both of which lead to larger increases of solute concentration in the PrCTF than those in the menisci during an interblink. Osmolarities for dry eyes are higher than those of normal eyes due to higher tear evaporation and lower tear production rates (Braun et al., 2015; Cerretani and Radke, 2014; Gaffney et al., 2010). Menisci hyperosmolarity correlates with dry eye (Farris, 1986; Farris et al, 1981, 1983; Gilbard, 1994; Gilbard et al., 1978; Lemp et al., 2011; Mathers et al., 1996; Mishima et al., 1971; Ogasawara et al., 1996; Tomlinson et al., 2006) because the salinity of the PrCTF in contact with the cornea influences that in the tear menisci through tear mixing upon blinking (Cerretani and Radke, 2014). Conversely, lack of significant correlation between osmolarity and dry eye seen by some studies (Amparo et al., 2014; Yeh et al., 2015) might be confounded by incomplete blinking, instrument limitation (Szalai et al., 2012), and/or lack of severe dry-eye patients recruited for the study (Yeh et al., 2015).

Gilbard et al. (1984) first documented the deleterious effects of hyperosmolarity on corneal epithelia using rabbit-eye cells both in vivo and in vitro. When cultured under hyperosmotic conditions, epithelial cells showed adverse responses including decreased intercellular connections, cell-membrane disruptions, and cellular swelling with decreased cytoplasmic density (Gilbard et al., 1984). In-vivo measurements displayed increased cell desquamation (Gilbard et al., 1984). Later, Gilbard et al. (1985, 1988) showed that tear hyperosmolarity also reduces corneal epithelial glycogen and increases conjunctival goblet-cell apoptosis. Studies on the ocular surface of mice (Luo et al., 2005) and on human limbal epithelial cells (Li et al., 2006) demonstrate that hyperosmolar stress activates mitogen-activated protein kinase pathways to produce proinflammatory cytokines, interleukin (IL) - 1β, tumor necrosis factor (TNF) α, and C-X-C chemokine IL-8. The effect of tear hyperosmolarity on ocular-surface immunology was accentuated by Guzmán et al. (2020) who established that tear hyperosmolarity initiates nuclear factor-κB signaling in conjunctival epithelial cells and increases dendritic cell recruitment and maturation. These authors also found that tear hyperosmolarity reduces the density of corneal intraepithelial nerves and terminals (Guzmán et al., 2020). Similarly, Hirata and co-authors (Hirata et al., 2013, 2014, 2015) revealed adverse effects of tear hyperosmolarity on corneal nerves of rats. Throughout their studies, Hirata et al. (2014, 2015) found that hyperosmolarity leads to corneal sub-basal nerve damage and disappearance of corneal-nerve responses that stimulate tear production. Moreover, those authors documented heightened sensitivity of nociceptive neurons to temperature after a hyperosmolar stress of only 15 min (Hirata et al., 2013). Liu et al. (2009) further showed that exposure of 700-mOsM aqueous salt to bovine corneal epithelial cells for 10–30 s activates mitogen-activated protein kinase (MAPK) pathways, demonstrating that the cornea reacts to a short-term hyperosmolar stress by exacerbating epithelial nerve firing. This observation provides strong evidence for corneal hyperosmolarity initiating dry-eye discomfort.

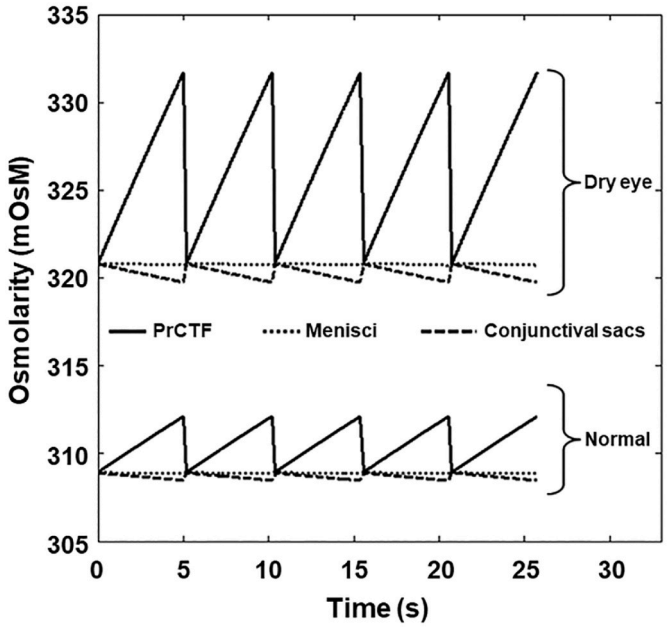

Fig. 1. Osmolarity of various tear compartments including pre-corneal tear film (PrCTF), menisci, and conjunctival sacs for normal and dry eyes with no-lens wear. Reprinted with permission from Cerretani and Radke. (2014). Copyright (2014) Taylor & Francis.

With soft-contact-lens (SCL) wear, the cornea is over laid by the post-lens tear film (PoLTF) and no longer is exposed to the environment where aqueous evaporation of the pre-lens tear film (PrLTF) increases interblink salinity. Because soft contact lenses experience minor displacements during blinking (Chauhan and Radke, 2001; Creech et al., 2001; Kok et al., 1992; Lin et al, 2003, 2006; McNamara et al., 1999), little mixing is expected between pre- and post-lens tear films (Lin et al, 2003, 2006; McNamara et al., 1999). Thus, at first glance, the PoLTF is isolated from the tear system and should protect corneal nerve endings from hyperosmolar stress. However, increased salt concentration in the PrLTF due to environment evaporation creates a concentration difference that drives salt across the lens and into the PoLTF. Thus, protection against PoLTF hyperosmolarity may not be complete.

Measurement of on-eye salinity in the approximately 2-μm thick PoLTF has not been achieved, although a number of groups have measured osmolarity associated with SCL wear (Chen et al., 2013; Golebiowski et al., 2017; İskeleli et al., 2002; Kojima et al., 2011; Martin, 1987; Sarac et al., 2012; Stahl et al., 2009). Unfortunately, reported lens-wear tear osmolarities are those of the tear meniscus (Chen et al., 2013; Golebiowski et al., 2017; Kojima et al., 2011; Martin, 1987; Sarac et al., 2012), combined tear of all tear compartments (Stahl et al., 2009), or total tear after lens removal (İskeleli et al., 2002). In view of these major limitations, it is not surprising that no association has been established between measured tear osmolarity and ocular comfort during SCL wear (Chen et al., 2013; Golebiowski et al., 2017; İskeleli et al., 2002; Sarac et al., 2012; Stahl et al., 2009). To date, the osmolarity of the PoLTF during SCL wear remains unknown despite the commonality of discomfort symptoms, including dryness, irritation, stinging, and burning, typically attributed to hyperosmolarity (Stapleton et al., 2013).

To determine whether a SCL can act as a barrier against osmolarity increases in the PoLTF, we quantify PoLTF tear osmolarity for differing physiological and lens properties with a tear-dynamics continuum mathematical model. Our proposed model extends the anterior tear-dynamics treatment of Cerretani and Radke (2014) to include a SCL and concomitant additional tear films. We incorporate deposition, interblink, and eye-closure phases of blinking as well as tear drainage, evaporation, and production that occur during these phases. The SCL tear-dynamics model also embodies tear exchange occurring between the PoLTF and pre-conjunctival tear films (PrCjTF) observed clinically with fluorophotometry (McNamara et al., 1999).

2. Tear dynamics

Fig. 2 illustrates the anterior ocular surface with SCL wear. The drawing is not to scale. The tear film interfacing the environment, either with lens wear (i.e., the PrLTF and PrCjTF) or without lens wear (i.e., the PrCTF and PrCjTF), evaporates during the interblink period. The thickness and cohesive quality of the meibomian-gland exuded tear lipid layer determine the volumetric tear evaporation rate (q_e) (Craig and

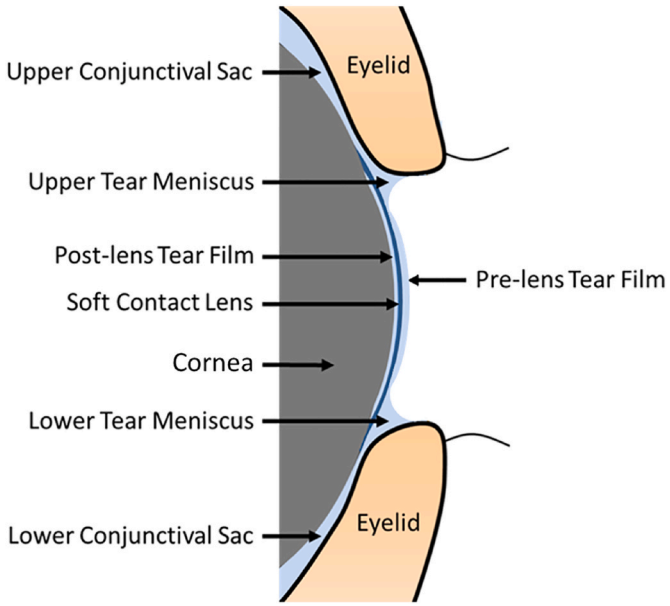

Fig. 2. Schematic of the ocular surface, tear-film compartments, and soft contact lens. Pre-conjunctival tear film is not visible in this cross-sectional view. The cornea is enveloped by the soft contact lens. The tear film interfacing the cornea is the post-lens tear film (PoLTF). Figure is not to scale.

Tomlinson, 1997). Due to black-line formation (McDonald and Brubaker, 1971; Miller et al., 2002), the tear film is "perched" during the interblink period (t_{ib}) and is effectively isolated from the two surrounding tear menisci (Miller et al., 2002). Consequently, evaporation of the tear film into the environment increases salt concentration and, subsequently, tear osmolarity (Siddique and Braun, 2015). Meanwhile, menisci osmolarity changes minimally due to the relatively large tear volume and smaller exposed surface area relative to the tear film. During contact-lens wear, the PrLTF evaporates but the lens prevents evaporation of the PoLTF. With zero PoLTF evaporation, the lens theoretically protects the ocular surface from increased salt concentration and, consequently, hyperosmolarity. However, increased salt concentration of the PrLTF due to evaporation creates a concentration gradient of salt, which leads to salt diffusion across the lens into PoLTF. The amount of salt that diffuses under this gradient depends on the lens-salt diffusivity (D_s), the lens-salt partition coefficient (k_s), and the lens thickness (h_{lens}) (Guan et al., 2011) among other variables, such as blink frequency, tear production rate, and evaporation rate. Conversely, diffusive supply of salt from the PrLTF into the PoLTF is opposed by an osmotic-pressure gradient that drives water across the lens from low to high salt concentration.

To quantify PoLTF tear osmolarity, anterior tear dynamics of the PrLTF, PrCjTF, PoLTF, tear menisci, and conjunctival-sac tear compartments all have to be accurately described. Alongside the tear compartments shown in Fig. 2, the tear-dynamics model must account for the three phases of the blink cycle: eyelid closure, interblink period, and deposition phase. These three major phases of the blink cycle are illustrated in Fig. 3. Behavior of each compartment during the blink cycle is summarized in the following subsections. Mathematical details are provided in Section 4, appendices, and augmented in Cerretani and Radke (2014).

2.1. Eyelid closure and opening

During eyelid closure, PrLTF, PrCjTF, tear menisci, and tear in conjunctival sacs mix. Due to the force of the eyelid, the PrLTF, PrCjTF, and tear menisci mix completely to reach a uniform tear osmolarity. However, the extent of fluid mixing in the conjunctival sacs with the PrLTF, PrCjTF, and tear menisci is unclear. With no-lens wear, a scintigraphic study showed that tracer inserted into the menisci rarely travels to the conjunctival sacs (Fraunfelder, 1976). Conversely, several fluorescence studies show that fluorescent dye in the upper and lower conjunctival sacs dilute to the rest of the tear after forceful blinking (Mishima et al., 1966; Tomlinson et al., 2009; Tomlinson and Khanal, 2005; van Best et al., 1995). Cerretani and Radke (2014) argued that the differences in mixing behaviors from the abovementioned studies are likely due to differences in blink strength and eye movement. Even if the tear compartments are not well mixed within a single blink, they will effectively mix with multiple blinks (Cerretani and Radke, 2014). Therefore, following the detailed discussion of Cerretani and Radke (2014), we argue that PrLTF, PrCjTF, tear menisci, and tear in conjunctival sacs are at a uniform salt concentration upon eyelid closure until the beginning of the subsequent blink during periodic steady state.

Although PrLTF, PrCjTF, tear menisci, and tear in the conjunctival sacs mix during an eye blink, the PoLTF does not mix well with the other tear compartments due to the SCL barrier. Two mechanisms that allow small amounts of tear exchange between PoLTF and the remaining tear

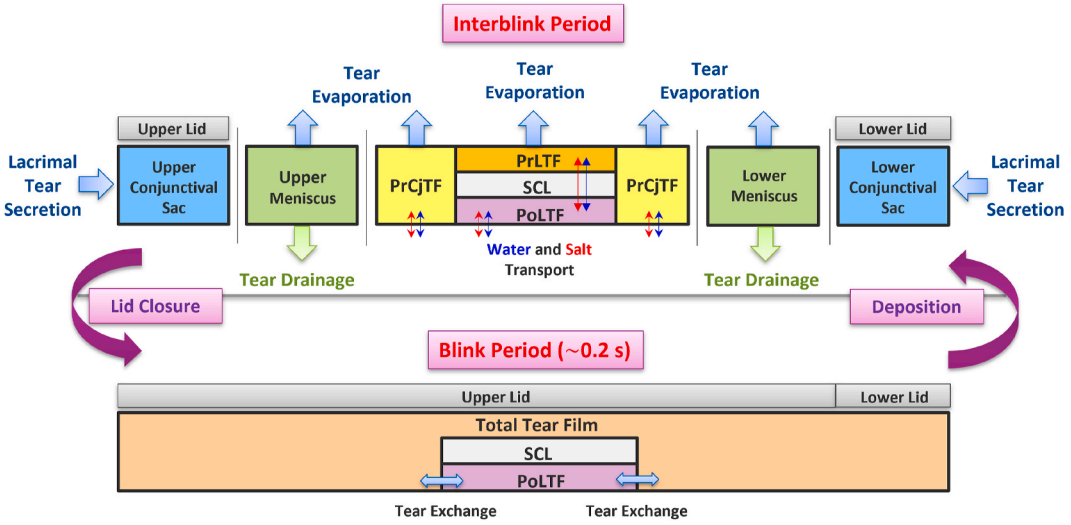

Fig. 3. Calculation flow diagram of anterior tear system behavior with soft contact lens (SCL) wear. Eyelid closure, interblink, and deposition phases are evident. Upper diagram illustrates open-eye period (5–30 s) while bottom diagram illustrates closed eye (~0.2 s). Salt flux from the bulbar conjunctiva to the PrCjTF is negligible and, therefore, is not included in the calculations. Figure is not to scale.

compartments are triggered by the force applied from the upper eyelid during a blink (Creech et al., 2001). The first type of tear exchange is induced by the lateral (up-down) motion of the lens due to the drag force during eyelid opening and closure. Through mathematical modeling, Chauhan and Radke (2001) predicted that lateral movement of the SCL during the blink phase varies depending on the lens elastic modulus and that the lens can move up to 3 mm vertically during a blink cycle.

The second type of tear exchange is caused by transverse (in-out) motion of the lens due to the normal force applied by the upper eyelid during a blink (Creech et al., 2001). This results in a lens pumping motion that squeezes out PoLTF fluid during eyelid closure and suctions in fresh fluid during eyelid opening, respectively. By using aqueous fluorescein isothiocyanate–dextran, McNamara et al. (1999) established that the net tear exchange between the PoLTF and rest of the tear compartments is 1–2% of the PoLTF volume per blink cycle. More exchange occurred with small diameter SCLs (i.e., 12.0 mm) than with larger diameter SCLs (i.e., 13.5 mm). McNamara et al. (1999) also determined that their tear-exchange values translated to 14.8–19.5 min to deplete 95% of the fluorescein from the PoLTF (T_{95}). For our tear-osmolarity analysis, 1% and 2% PoLTF volume tear exchanges per blink were addressed. Tear osmolarity differences using the two exchange percentage volumes proved negligible for all tear compartments. We set the PoLTF thickness upon eye opening at 2 μm following tear mixing where 1% of the eye-opening PoLTF volume is tear introduced from tear exchange. We chose the 1% PoLTF volume for tear exchange because currently available SCLs have somewhat larger diameters (e.g., 13.8–14.5 mm) than the largest diameter SCL (i.e., 13.5 mm) examined by McNamara et al. (1999).

2.2. Tear deposition

During eye opening, the rising upper-lid meniscus deposits a thin tear film on the surface of the contact lens and surrounding basal conjunctiva to form the PrLTF and PrCjTF, respectively (Wong et al., 1996). Similar to the PrCTF, the PrCjTF consists of a mucin-rich region, an aqueous interlayer, and a thin lipid layer (Willcox et al., 2017). Because of the interposed contact lens, the PrLTF is no longer exposed to corneal glycocalyx and corneal mucin-producing goblet cells (Craig et al., 2013). The lipid layer covering both the PrLTF and PrCjTF is secreted by the lid meibomian glands (Cedarstaff and Tomlinson, 1983) while the majority of the aqueous layer is produced from the lacrimal glands (Dartt and Willcox, 2013). Tear production is discussed more in depth in Section 2.3.

The thicknesses of the tear films deposited on the conjunctiva and the lens surface depend on the upper tear-meniscus radius (R_{um}) and the relative upper-eye-lid velocity (Cerretani and Radke, 2014; Wong et al., 1996). Mathematically, the relationship of PrCjTF or PrLTF thicknesses to upper-tear meniscus radius and relative velocity is obtained from Bretherton (1961) and extended from that of Cerretani and Radke (2014) to include the effect of a SCL.

$$h_{tf,j} = 1.34 R_{um} \left[\mu_w \left(u_{lid} - u_{s,j}\right) / \gamma\right]^{2/3} \quad (1)$$

where $h_{tf,j}$ is the thickness of PrCjTF or PrLTF at the beginning of the interblink period, subscript j indicates whether the film is PrCjTF ($j = PrCj$) or PrLTF ($j = PrL$), μ_w is tear viscosity, u_{lid} is the velocity of the upper lid, $u_{s,j}$ is the velocity of the bulbar conjunctiva ($j = PrCj$) or the contact lens ($j = PrL$) during eye opening, and γ is tear surface tension. Since the bulbar conjunctiva does not move during a blink, $u_{s,PrCj}$ is zero when determining the thickness of PrCjTF. Conversely, the upward velocity of the contact lens is nonzero due to the drag force exerted by the eyelid on the lens as determined from the lens-displacement analysis of Chauhan and Radke (2001). Parameter values used to determine the tear-film thicknesses at the start of the interblink period are provided in Table 1. Tear surface tension has been measured by multiple groups with significantly different results (Nagyová and Tiffany, 1999; Svitova and Lin, 2010; Tiffany et al., 1989). Variability is understandable because of the complex procedure to collect human tear and lipid for ex-vivo study and because of the dynamic nature of lipid spreading. We employ the higher tension value of Tiffany and co-authors (Nagyová and Tiffany, 1999; Tiffany et al., 1989) in Table 1 since surface tension is expected to be higher near the upper meniscus during lid opening.

Table 1
Tear, lid, and palpebral aperture parameters.

PARAMETER	SYMBOL	VALUE (UNIT)
Tear viscosity	μ_w	1.5[a] $(mPa \times s)$
Tear surface tension	γ	45[b] (mN/m)
Upper Eyelid Velocity	u_{lid}	0.05[c] (m/s)
Contact Lens/Conjunctiva Velocity	$u_{s,j}$	0.02[c]/0 (m/s)

[a] Obtained from Ehlers (1965) and Tiffany (1991).
[b] Obtained from Nagyová and Tiffany (1999) and Tiffany et al. (1989).
[c] Derived from Chauhan and Radke (2001).

Because of the upward motion of the lens during a blink, the PrLTF is thinner than the PrCjTF or the PrCTF. This result is supported by the measurements of Wang et al. (2003), who found PrLTF thicknesses after lens fitting to be 3.6 ± 2.1 μm and PrCTF thicknesses to be 4.7 ± 2.3 μm, and King-Smith and his co-authors, who found PrLTF thicknesses of 2.3 ± 0.8 μm (Nichols and King-Smith, 2003) and PrCTF thicknesses of 2.7 ± 0.4 μm (King-Smith et al., 2000). A thinner PrLTF compared to the PrCTF suggests earlier tear-film breakup over a SCL compared to breakup over the cornea (McMonnies, 2020; Nichols et al., 2005).

2.3. Tear production

Volumetric aqueous production rate (q_{lac}), tear drainage rate (q_d), and tear evaporation rate (q_e) strongly regulate tear osmolarity. The lacrimal glands produce the vast majority of the aqueous fluid of the tear (Dartt and Willcox, 2013). In comparison, the cornea and conjunctiva provide relatively small amounts of aqueous fluid (Dartt and Willcox, 2013). Without lens wear, lack of sufficient aqueous production from lacrimal glands results in aqueous-deficient dry eye (Stern et al., 2004; Sullivan, 2004). A decreased aqueous-tear-layer volume leads to a more rapid increase in osmolarity upon tear evaporation. Glasson et al. (2006) determined that wetted lengths of phenol-red threads were not statistically different with and without lens wear. In the same study, Glasson et al. (2006) showed that intolerant SCL wearers produced shorter wetted lengths than those for tolerant SCL wearers. Unfortunately, measured wetted lengths are not an accurate representation of q_{lac} because the tear volume within the tear lake and the aqueous evaporation from the thread are not accounted for in the phenol-red thread test (Li et al., 2018). We assume the same tear production rate with lens and no-lens wear because to date there are no substantiated differences in aqueous production rates.

Until recently, direct clinical measurement of q_{lac} was not available. Accordingly, Cerretani and Radke (2014) used available literature data (Khanal et al., 2008, 2009; Tomlinson and Khanal, 2005) for q_e, tear turnover rate, tear volume, and lower meniscus osmolarity (c_{lm}) to back calculate q_{lac}. Since then, significant effort was directed towards modifying the Schirmer tear test to quantify q_{lac} directly (Kim et al., 2019; Li et al., 2018; Telles et al., 2017). In a limited clinical study, Kim et al. (2019) established a mean q_{lac} of 1.19 μL/min for 17 subjects. The inter- and intra-subject variability of q_{lac} was significant and q_{lac} did not exceed 2.2 μL/min. This observation is consistent with the calculated values of Mishima et al. (1966) from tear-turnover rates. However, Kim et al. (2019) could not determine q_{lac} from dry-eye subjects that did not wet the Schirmer strip past 5 mm within the 5-min testing time. Therefore, the determined mean q_{lac} excludes the data of those dry-eye subjects and is likely closer to that of normal eyes. Since the measured mean q_{lac} of Kim et al. (2019) is very similar to that calculated for normal eye by Cerretani and Radke (2014), we simply used the q_{lac}

values of normal and dry eyes determined by those authors as listed in Table 2. Details of how q_{lac} was determined are provided in Appendix D of Cerretani and Radke (2014). We also incorporate the small rates of corneal and conjunctival tear production following the work of Cerretani and Radke (2014).

2.4. Tear drainage

By using high-speed photography, Doane (1981) visualized and explained tear drainage during blink cycles. Upon eyelid closure, the upper eyelid sweeps downward to consolidate tear film into the lower meniscus, while the lower eyelid moves laterally in the nasal direction to deliver tear in the lower meniscus into the medial canthus for eventual tear drainage (Doane, 1981). During the first ~1/3 of lid closure, upper and lower puncta are occluded by the lid margins. The remaining 2/3 of eyelid closure squeezes tear in the canaliculi and lacrimal sac into the nasal cavity through the nasolacrimal canal. When the eyelid retracts, relaxation of canaliculi and lacrimal sac lowers the liquid pressure below that of the environment. Consequently, once the eye opens and the puncta are no longer occluded, tear in the medial canthus is sucked into the puncta by capillary action filling the canaliculi and lacrimal sac and restoring liquid pressure. Thus, tear drainage from the ocular surface occurs during the interblink and depends on the tear-meniscus radii and blink strength.

Tomlinson and Khanal (2005) estimated tear-drainage rate by clinically measuring the tear-turnover rate upon instilling aqueous fluorescein dye into the eye and following the reduction in fluorescein intensity. With known initial fluorescein concentration, volume of the fluorescein drop, and transient decline in fluorescein intensity, tear-drainage rate can be calculated. This method, however, is indirect, assumes that the tear volume remains constant, and requires a correction factor for the fluorophotometer (Tomlinson and Khanal, 2005). Tear-turnover rates from various authors tabulated by Tomlinson and Khanal (2005) ranged from 0.12 to 1.47 μL/min.

Based on Doane's observations (Doane, 1981), Zhu and Chauhan (2005) developed a sophisticated mathematical tear-drainage model recognizing that the drainage rate through the puncta arises primarily from capillary suction. They established that the range of drainage rates for normal eyes is rather large from 0.10 to 4.00 μL/min depending on the canaliculus thickness and Young's modulus. Subsequently, Cerretani and Radke (2014) simplified the Zhu and Chauhan (2005) analysis by relating the capillary-pressure-driven drainage rate to the upper and lower menisci radii. We utilize the formulation of Cerretani and Radke (2014) here for our q_d estimates. Although q_d ranged from 0.10 to 4.00 μL/min for the model of Zhu and Chauhan (2005), the semi-empirical model of Cerretani and Radke (2014) ranged q_d from 0 to 2.00 μL/min since tabulated tear-turnover rates of Tomlinson and Khanal (2005) suggest that tear-drainage rates do not exceed 2.00 μL/min. Further information can be found in Section 4.2.1.

2.5. Tear evaporation

Upon completion of eye opening, PrCjTF, PrLTF, and tear menisci are exposed to the environment and undergo evaporation, thereby increasing compartment tear osmolarities. Similar to no-lens wear, lens-wear q_e is affected by the quantity and quality of the tear-lipid layer (Cedarstaff and Tomlinson, 1983) in addition to environmental factors, such as surrounding temperature, airflow, and humidity (Rolando and Refojo, 1983). McCully and Shine (1997) suggested a lamellar-stack structure for the lipid layer that is approximately 10 nm in thickness. Observed colors in the spreading lipid layer (Korb et al., 1998) and the in-situ interferometry measurements of King-Smith et al. (2010), however, indicate a much thicker layer, greater than about 50 nm. Rosenfeld et al. (2013) found that fully organized lamellar structure is not consistent with the discrete melting behavior found in their rheologic, x-ray scattering, and differential scanning calorimetry studies. Instead, a duplex-film waxy-suspension structure of 50–100 nm in lipid-layer thickness was proposed. Although retardation of q_e by the lipid layer has been well documented (Cedarstaff and Tomlinson, 1983; Craig and Tomlinson, 1997), the molecular architecture of the lipid layer and how much it reduces tear evaporation are not settled.

As reviewed by Tomlinson et al. (2005, 2009), most studies of in-situ tear evaporation use closed-chamber evaporimeters that are misinterpreted as well mixed in both temperature and relative humidity. Interferometry measurement of tear film thinning under open air and under a goggle by Kimball et al. (2010) further suggest that closed-chamber evaporimeters do not provide accurate measurement of tear-film evaporation. To overcome the well-mixed deficiency and to quantify the role of room air circulation, Peng et al. (2014b) developed an in-vivo flow evaporimeter that quantifies the effects of airflow velocity and relative humidity while measuring environmental temperature. Fig. 4 illustrates the device. Inlet air of known relative humidity, R_H, temperature, and volumetric air flow, Q, gently impinges on the eye where tear evaporation humidifies the outlet flow stream. The rate of tear evaporation is calculated from the measured humidity increase of the return air. In a limited three-subject analysis, they showed that increasing the inlet relative humidity from 20 to 40% resulted in up to a 40% decline in q_e and varying the airflow velocity from 5 to 16 cm/s resulted in up to 50% increase in q_e. The preliminary clinical results of Peng et al. (2014b) at the lowest flow velocities fall within the rather wide range of q_e values tabulated by Tomlinson et al. (2005, 2009). This finding accentuates the need for q_e measurements with well-defined airflow and relative humidity. For our tear-system calculations, q_e values without lens wear for both normal and dry eyes were averaged from the groups tabulated by Tomlinson et al. (2005, 2009) along with the data from Peng et al. (2014b) at a relative humidity of 40% following the procedure of Cerretani and Radke (2014). Table 2 gives the resulting values.

Effects of long-term contact-lens wear on meibomian-gland health and, hence, on tear evaporation are debated. Arita et al. (2009) documented a decrease in the number of functional meibomian glands and Alghamdi et al. (2016) noted frequent dropout of meibomian glands in lens wearers. Conversely, Machalińska et al. (2015) and Ong (1996) found no correlation between contact-lens wear and meibomian-gland health. Guillon and Maissa (2008) found 40–50% higher tear evaporation rates of lens wearers than those of non-lens wearers. Similarly, a 5-subject study of Cedarstaff and Tomlinson (1983) saw an increase in q_e with lens wear. Conversely, Hamano et al. (1981) reported both increases and decreases in q_e with lens wear among their 10-subject study using a closed-chamber evaporimeter. We adopt the 50% increase in lens-wear tear evaporation rate of normal subjects suggested by Guillon and Maissa (2008) and listed in Table 2. To our knowledge, q_e of the PrCjTF and the PrLTF have not yet been separately measured. Therefore, we assume here that they are identical.

Table 2
Tear production and evaporation rates.

CASE	LACRIMAL PRODUCTION RATE (q_{lac})	TEAR EVAPORATION RATE (q_e)
Normal (μL/min)	1.10	0.15
Dry Eye (μL/min)	0.55	0.30
Normal Lens Wear[a] (μL/min)	1.10	0.23

[a] Determined based on measurements of Guillon and Maissa (2008) with 30–40% relative humidity.

2.6. Soft contact lens

Simultaneous water and salt transport occur between the PrLTF and the PoLTF because SCL materials are both water (Boushehri et al., 2010) and salt permeable (Guan et al., 2011). Salt concentration differences,

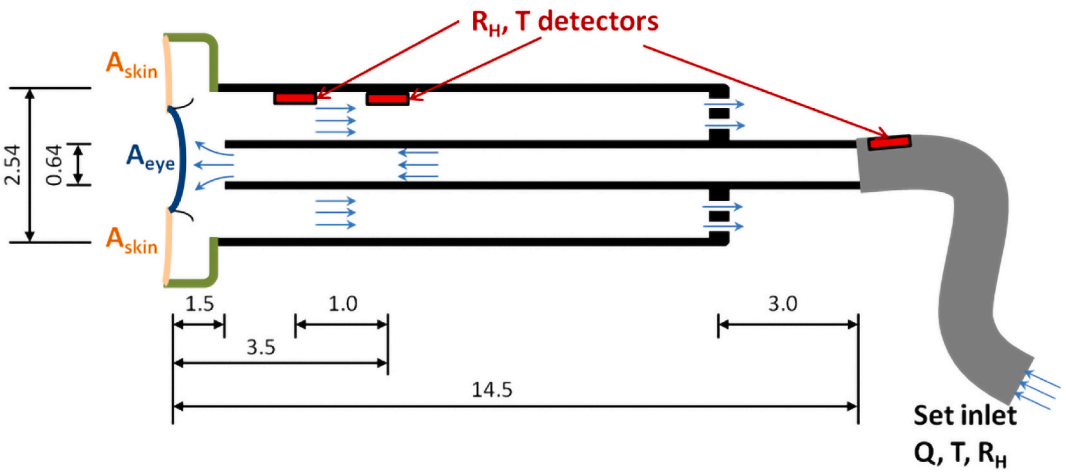

Fig. 4. Schematic of flow evaporimeter. At a set air flow volumetric rate, Q, inlet and exit relative humidities, R_H, and temperatures are measured permitting calculation of evaporation rate. Dimensions are in cm. Drawing is not to scale. Reprinted with permission from Peng et al. (2014b). Copyright (2014) American Chemical Society.

which occur across the SCL due to PrLTF evaporation, and lens properties (i.e., D_s, k_s, and h_{lens}) determine the rate of salt transport across the lens. Salt transport occurs from high to low concentration whereas simultaneous water transports in the opposite direction due to the osmotic-pressure difference.

The rate of water transport through the lens depends on h_{lens}, on water viscosity, and on the hydraulic permeability of water (K) (Monticelli et al., 2005). Because of the difference in deposited tear-film thickness between the PrLTF and the PrCjTF during lens wear, there also exists a lateral salt-concentration difference between these two regions to cause water and salt transport at the lens landing zone where the PrLTF interfaces with the PrCjTF. Potential impacts of salt and water transport between different tear compartments and across the SCL are further discussed in Section 5.

For salt transport, D_s describes how fast salt travels within a SCL material, whereas k_s describes the ability for salt to partition into the lens material at the SCL/tear-film interfaces when in equilibrium with a given aqueous salinity. In steady state, D_s and k_s appear as the product of the two as the salt permeability, D_sk_s. Because our tear system is dynamic, values for both D_s and k_s are required separately in this study (Peng and Chauhan, 2012). Yasuda et al. (1968) established that an increase in water content of a cross-linked hydrogel increases both D_s and k_s. Therefore, in Section 3 to follow, we determine individual lens properties (D_s, k_s, and K) necessary to quantify lens salt and water transport rates.

2.7. Perched tear film

From both a clinical in-vivo study using aqueous fluorescein and an in-vitro study, McDonald and Brubaker (1971) showed that the tear film near the tear menisci thins due to a Young-Laplace (Berg, 2009) pressure difference between the concave menisci and the less curved tear film during an interblink period. Thus, a lower liquid pressure exists in the curved menisci compared to that in the less curved convex tear film because of surface tension and the curvature difference of the air/liquid interface (Maki et al., 2010; Miller et al., 2002). The resulting capillary pressure difference drives flow from the tear film into the menisci. The flow resistance in the thin tear film is strong enough for the capillary-pressure suction to create a thin dimple in the tear film directly adjacent to menisci immediately upon stoppage of the upper eyelid opening (Miller et al., 2002). When viewed under fluorescein instillation, the thin dimples appear as "black lines" (McDonald and Brubaker, 1971; Miller et al., 2002) due to quenching of the fluorescein (Finnemore et al., 1998). Black lines effectively isolate the tear film from mixing with the menisci leading to so-called "perched" tear films (Fatt, 1991; Miller et al., 2002). Thus, evaporative salinity increases in the tear film are not diluted by mixing with the connecting menisci.

However, based on clinical observations of one of our co-authors (MCL), not all subjects display visible black lines after fluorescein insertion. This may be caused by conjunctival folds preventing formation of meniscus concavity and a smaller pressure difference between the menisci and the adjacent convex tear films. In such cases, there is a possibility that the tear film is not strongly isolated during the interblink period. We deal with this situation in Appendix E and establish that salt exchange between the PrLTF and the menisci has negligible effect on the determined compartment osmolarities.

With SCL wear, black lines are not observable due to dye solubility in the lens obscuring black-line visualization (Refojo et al., 1972). Numerous studies have reported and quantified concave tear menisci with SCL wear (Chen et al., 2011; del Águila-Carrasco et al., 2015; Tao et al., 2011; Wang et al., 2009). This observation plus the very low hydraulic permeability of SCLs indicate that the PrLTF can also be considered as perched during an interblink.

Proceeding Sections 3 and 4 provide detail on the lens transport-property measurements and on the tear-system modeling mathematics. Readers interested in results may proceed to Section 5.

3. Lens-transport properties

With the advent of silicone-hydrogel SCLs to minimize corneal hypoxia during lens wear, considerable effort has been made to determine water and salt transport coefficients across SCLs (Boushehri et al., 2010; Guan et al., 2011; Hoch et al., 2003; Monticelli et al., 2005; Nicolson et al., 1999; Peng and Chauhan, 2012). We now outline the experimental measurements that set the transport parameters of the SCL pertinent to assess PoLTF salinity during contact-lens wear. Salt and water transport are discussed separately.

3.1. Salt transport

Lens-salt permeability, D_sk_s, is directly measured in a modified Stokes cell: a two-chamber system separated by the SCL (Guan et al., 2011; Mann et al., 2019; Nicolson et al., 1999; Peng and Chauhan, 2012). A schematic of the apparatus developed by Guan et al. (2011) is highlighted in Fig. 5. The bottom chamber of the apparatus is initially filled with a salt-water solution of known concentration while the top chamber is initially filed with deionized water. Both chambers are well stirred to eliminate mass transfer resistances at each side of the lens. By

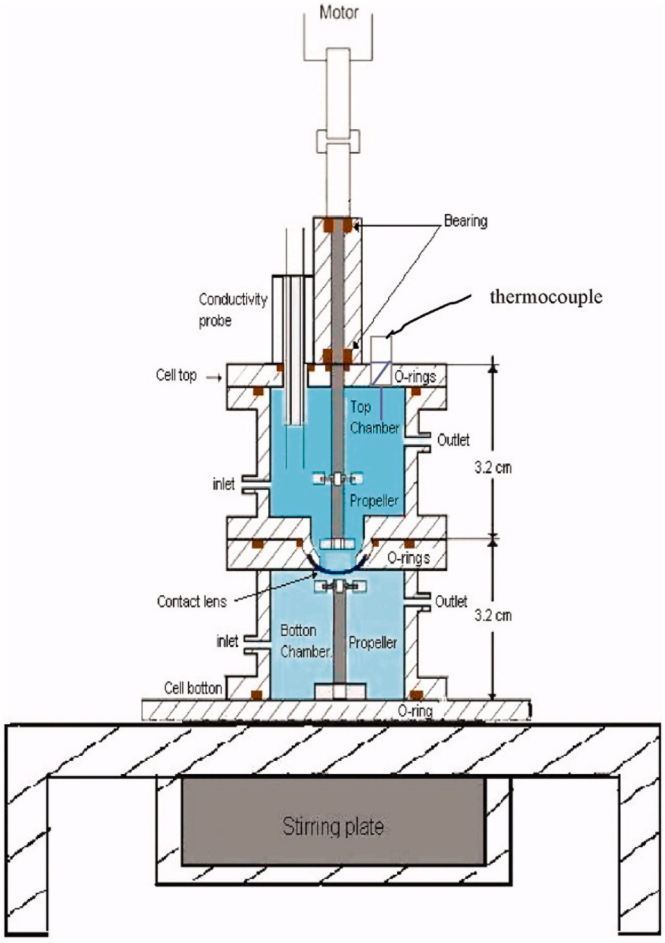

Fig. 5. Schematic of the Stokes cell developed by Guan et al. (2011) to measure the salt permeability ($D_s k_s$) of SCLs. Bottom chamber has a known initial salt concentration while the top chamber is initially filled with deionized water. Electrical conductivity determines the rise in salt concentration of the top chamber. Reprinted with permission from Guan et al. (2011). Copyright (2011) John Wiley and Sons.

detecting the electrical conductivity in the top cell over time and by invoking pseudo-steady salt diffusion across the lens, the value of $D_s k_s$ is obtained directly (Guan et al., 2011; Peng and Chauhan, 2012). To garner individual values of D_s and k_s, both Guan et al. (2011) and Peng and Chauhan (2012) measure the equilibrium partition coefficient in a separate back-extraction experiment. A lens of known dry mass is first soaked in an aqueous solution of known high salt concentration until equilibrium is reached. The salt-equilibrated lens is then placed in well-mixed deionized water where salt leaches out until a new equilibrium is attained. k_s is calculated from the difference in initial and final equilibrium leached-salt concentrations by mass conservation. Once k_s is known, lens-salt diffusivity follows from the Stokes-cell measured salt permeability.

Alternatively, Peng and Chauhan (2012) extend the back-extraction procedure by monitoring the leached salt concentration in time until equilibrium emerges. The time course of the leached salt concentration is fit to Fick's second law to establish D_s. The salt partition coefficient, k_s, is ascertained by the back-extracted equilibrium concentration as above; salt permeability is then given by the product of D_s and k_s. These authors found that the pseudo-steady Stokes-cell and the transient back-extraction methods give comparable results.

Fig. 6 shows measured equilibrium salt partition coefficients of 1 M NaCl in silicone-hydrogel (open symbols) and HEMA-based (filled symbols) SCLs as a function of lens fractional water content reproduced

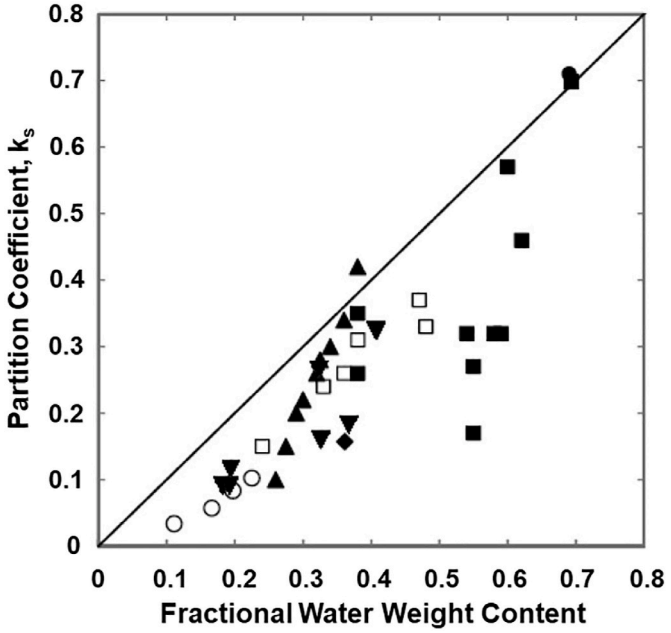

Fig. 6. Partition coefficient, k_s, versus fractional water weight content at 35°C. Open symbols correspond to silicone-based material lenses (SiHy) and filled symbols represent hydroxyethyl-methacrylate-based material lenses (HEMA). Rectangles represent commercial lenses while other symbols represent hydrogel membranes studied from various authors. The solid line corresponds to when the partition coefficient equals the lens water content. Reprinted with permission from Guan et al. (2011). Copyright (2011) John Wiley and Sons.

with permission from Guan et al. (2011). The solid line corresponds to a partition coefficient equaling the water content of the lens. Except at high water contents, salt partitioning into SCLs falls below this simple relationship.

Guan et al. (2011) and later Dursch et al. (2014) note that ideal salt partitioning into hydrogels corresponds to $k_s = \phi_w$ where ϕ_w is the water volume fraction in the lens. Deviations from ideal partitioning are accounted for by introducing a salt-enhancement factor: $E_s (\equiv k_s/\phi_w)$. Dursch et al. (2014) suggest that the enhancement factor is the product of at least three contributions $E_s = E_s^{ex} E_s^{el} E_s^{ad}$ where E_s^{ex} designates hard-sphere exclusion from the gel, E_s^{el} reflects nonspecific electrostatic repulsion or Donnan exclusion, and E_s^{ad} corresponds to specific adsorption of salt to the polymer chains of the gel. The small deviations from ideality in Fig. 6 and the high ionic strength of the aqueous salt solution dictate that the electrostatic-repulsion factor is close to unity. We do not expect strong specific adsorption of salt to the lens polymeric strands so the adsorption enhancement factor is also unity. Thus, partial rejection of salt from the SCLs in Fig. 6 suggests hard sphere repulsion exclusion so that E_s^{ex} is slightly less than unity. Calculations in Guan et al. (2011) and Dursch et al. (2014) reveal that this suggestion is reasonable and that $k_s = \phi_w$ at large water contents consistent with Fig. 6.

Fig. 7 reports measured aqueous salt diffusion coefficients in SCLs as a function of inverse water content from the work of Guan et al. (2011). As in Fig. 6, open symbols correspond to silicone-hydrogel lenses and filled symbols correspond to HEMA-based lenses. As water content decreases, salt diffusivity in the lenses decreases by orders of magnitude from its value in water. Solute diffusivities in hydrogels relative to that in bulk water can be expressed as the product of a hydrodynamic resistance factor, F, and an obstruction factor, S: $D_s/D_\infty = FS$ (Brady, 1994; Dursch et al., 2014). Here, D_∞ represents bulk molecular diffusion coefficient of aqueous sodium chloride. The myriad of small cross-linked polymer strands in swollen hydrogels causes both hydrodynamic and obstruction factors to be considerably smaller than unity. Several theories for diffusion in hydrogels suggest that $D_s/D_\infty = \exp[-a(1-\phi_w)^b]$

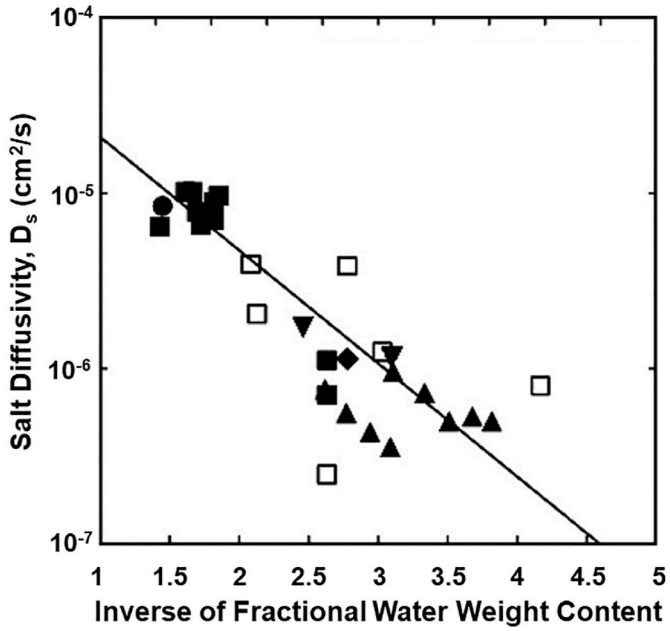

Fig. 7. Semilogarithmic graph of salt diffusivity, D_s, versus the inverse fractional water weight content at 35° C. Horizontal axis of unity corresponds to the diffusivity of salt in pure water at 35° C. Open symbols correspond to silicone-based material lenses (SiHy) and filled symbols represent hydroxyethyl-methacrylate-based material lenses (HEMA). Squares represent commercial lenses while other symbols represent hydrogel membranes studied from various authors. The solid line guides the eye. Reprinted with permission from Guan et. (2011). Copyright (2011) John Wiley and Sons.

where a and b are adjustable constants (Amsden, 1998). For $b = 1$, Yasuda et al. (1968) demonstrate that for large water contents this expression can be rewritten as $\ln(D_s/D_\infty) = -a[\phi_w^{-1} - 1]$. If we approximate water volume fractions in the lenses by lens water content, the eye-fit straight line in Fig. 7 confirms this relationship. Another way of understanding the strong reductions in salt diffusion coefficients by SCLs is from the expression $D_s = D_\infty/\tau_s^2$ (Guan et al., 2011) where τ_s is the lens-salt tortuosity or the ratio of path length taken by the salt ions as they traverse through the gel to the gel thickness. According to Table III of Guan et al. (2011), τ_s in SCLs varies from 2 to close to 10 or reductions in aqueous salt diffusivities by up to 100, consistent with Fig. 7. D_s values adopted in this manuscript were chosen based on the values of Guan et al. (2011) and of Mann et al. (2019) for more modern SCLs.

3.2. Water transport

Hydrodynamic permeability, K, of a SCL for pressure-driven aqueous flow is necessary to predict osmotic-pressure back flow through a lens exposed to a salt concentration difference. We rely on the values measured by Monticelli et al. (2005). Fig. 8a is a schematic of the apparatus. Water is forced through the membrane by an air-pressure-driven constant-head tank. Volumetric flow rate is measured by the water-height change rate in the small-diameter vertical capillary tube. Flow rates through the SCL membrane sheets are very small requiring data collection over many hours. With such small flows, care must be taken to prevent leakage around the membrane. Fig. 8b displays the membrane-holder design and the requisite O-ring seals. With the pressure drop and volumetric flow rates measured for varying applied pressure drops, and with the known water viscosity, thickness of the membrane, and membrane cross-sectional area, K follows from Darcy law (Brenner and Edwards, 1993): $v_w = (K/\mu_w)[-\Delta P/L]$ where v_w is superficial velocity, μ_w is tear viscosity, L is membrane thickness, and ΔP is pressure drop. Defined in this manner, the units of hydraulic permeability are length squared: K equal to 1 Darcy, characteristic of beach sand, corresponds to 1 μm^2.

Fig. 9 from Liu et al. (2013) reports K values as a function of $(1-\phi)^3/\phi^2$ from Monticelli et al. (2005) and Refojo (1965) at typical water contents of SCLs and Quinn and Grodzinsky (1993) for hydrogels of much higher water contents where ϕ is the polymer volume fraction in the lens. Liu et al. (2013) write the functionality of K with polymer content as

$$K = \frac{(1-\phi)^3}{8\phi^2\tau_H^2}a_f^2 \tag{2}$$

where a_f is the polymer-strand characteristic radius and τ_H is the hydrodynamic tortuosity. Equation (2) motivates the $(1-\phi)^3/\phi^2$ choice for the abscissa in Fig. 9. On log-log axes, Equation (2) demands a straight line and allows calculation of a_f/τ_H. Liu et al. (2013) identify a strand radius of around 2 nm and a hydrodynamic tortuosity of about 5, in general agreement with those above for salt-diffusion tortuosities determined by Guan et al. (2011). An important finding from Fig. 9 is the extremely small SCL hydrodynamic permeabilities in the pico-Darcy range. The reason for these small valves is the very small molecular polymer fiber size.

4. Mathematical formulation

In this section, we outline the isothermal tear-dynamics model with SCL wear for time-periodic blinking. To predict tear osmolarity in the PoLTF, PrLTF, PrCjTF, and tear menisci with SCL wear, water and salt mass must be conserved in all tear compartments during blink and interblink periods. We assume that the properties of salt are those of aqueous sodium chloride, which is the dominant solute in tear. The proposed model accounts for PrLTF evaporation, tear exchange at the lens periphery, tear-film deposition, lacrimal-gland tear production, tear drainage, water and salt fluxes through the SCL, and tear production from the cornea and conjunctiva. All calculations are performed in Matlab R2019b (Mathworks, Natick, MA). Computation of the three phases of the blink cycles (i.e. deposition period, interblink period, and eyelid closure) are repeated until periodic-steady state is attained. We assess the importance of lens parameters (i.e., D_s, k_s, K, and h_{lens}), duration of interblink period (i.e., t_{ib}), and tear evaporation and production (i.e., q_e and q_{lac}) on tear-film compartment osmolarities. Fundamental equations are summarized in the following subsections while detailed equations are available in the appendices or in the work of Cerretani and Radke (2014).

4.1. Deposition phase

The tear-deposition period involves formation of upper and lower menisci, PrLTF, and PrCjTF during upper-lid rise. Due to the short time ~0.2 s interval of the deposition phase, we assume that evaporation is negligible. At the beginning of deposition, the initial tear volume and salt concentration of the menisci are determined iteratively so that the mass of salt and water are conserved in all tear compartments. This calculation is unchanged from that of Cerretani and Radke (2014) (see Appendices B and D of that reference).

Due to upward lens motion during eye opening (Chauhan and Radke, 2001), deposited film thicknesses are different in the PrLTF (lens region) and PrCjTF (no-lens region) as determined from Equation (1). Consequently, upon completion of PrLTF and PrCjTF deposition, upper meniscus volume and curvature radius differ between the PrLTF and PrCjTF regions. As the meniscus-volume difference between the two regions is small and has minimal effect on the meniscus osmolarity during the interblink period, the two upper-meniscus volumes are averaged to determine an average upper-meniscus radius.

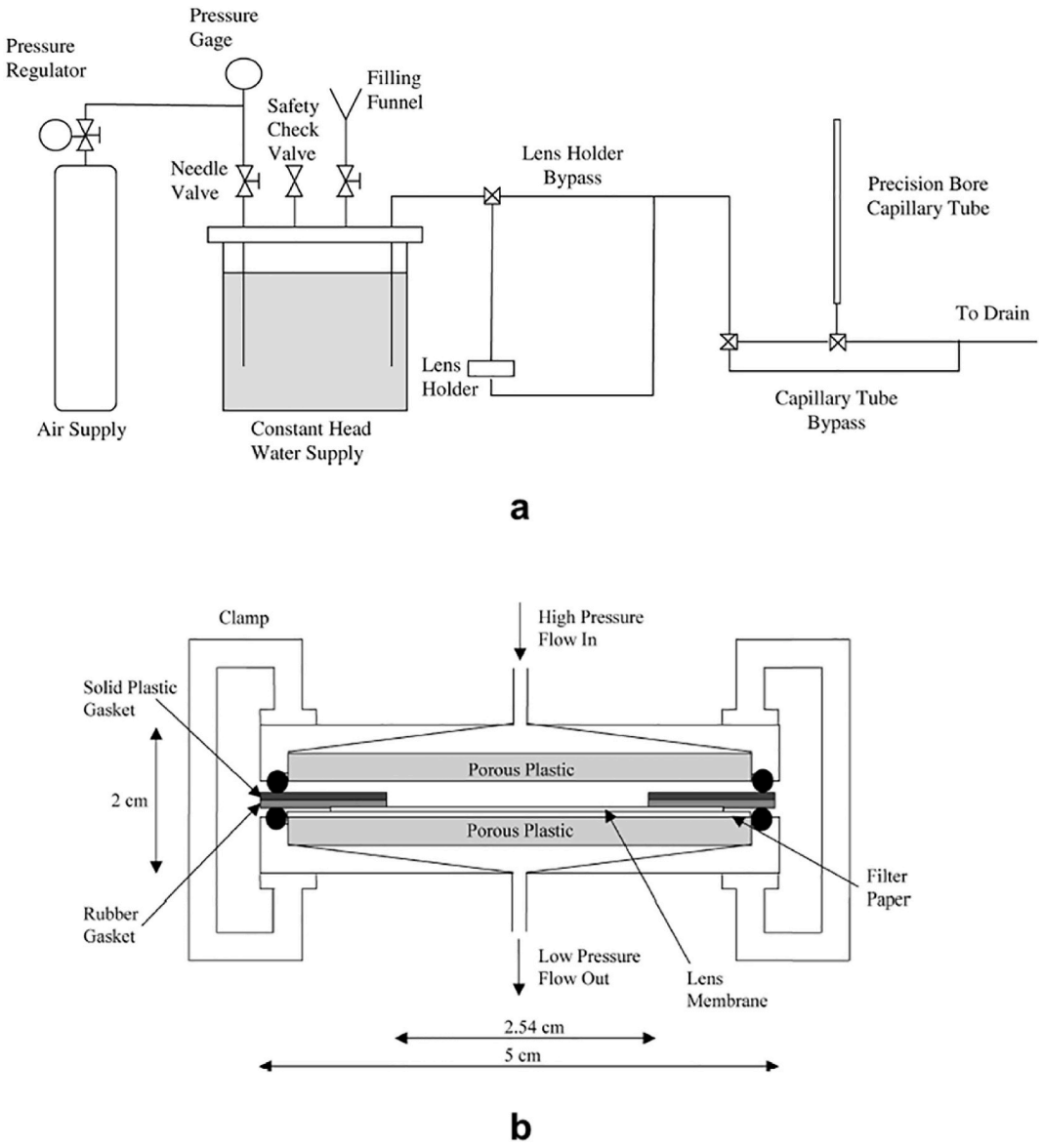

Fig. 8. Schematic of the flow apparatus to measure Darcy hydraulic permeability, *K*, of a SCL membrane. (a) Overall design and (b) detailed design of the lens-membrane holder are provided. Water is forced through the lens membrane that is placed in the lens-membrane holder by a known pressure difference. Water rise in vertical capillary tube allows determination of the volumetric flow rate to measure *K*. Reprinted with permission from Monticelli et al. (2005). Copyright (2005) Taylor & Francis.

4.2. Interblink period

During the interblink period, the transient partial differential equation for transport across the lens is solved numerically with forward finite difference (Newman and Thomas-Alyea, 2004). Meanwhile, the time-dependent ordinary differential equations for the compartment mass balances are solved with a Runge-Kutta marching algorithm (ode45 command in Matlab) following the work of Cerretani and Radke (2014). Ordinary differential equations are converged every time step of 0.01 s until periodic steady state is reached. Except for the SCL, we assume that each tear compartment is well mixed during the interblink period. Mathematical representation of salt and water transport for each compartment is provided below. Required physical constants are provided in Table 3. Values for physical constants not specifically listed and details regarding the numerical methodology are available elsewhere (Cerretani and Radke, 2014; Newman and Thomas-Alyea, 2004).

4.2.1. Tear menisci

In the interblink period, tear flows into the upper and lower menisci from the upper and lower conjunctival sacs, respectively. Following Cerretani and Radke (2014), 80% of q_{lac} flows into the upper conjunctival sac from the lacrimal gland while the remaining 20% of q_{lac} flows into the lower conjunctival sac. Meanwhile, tear also drains from the menisci via capillary suction through the puncta (Cerretani and Radke, 2014; Doane, 1981; Zhu and Chauhan, 2005). Water conservation for each tear meniscus is written as

$$\frac{dV_{im}}{dt} = q_{laci} - q_{di} - q_{e,im} \qquad i = u, l \quad (3)$$

where $i = u$ or l to denote upper or lower meniscus, respectively, t is time, $V_{im} = 2(1 - \pi/4)R_{im}^2 S_{lid}$ is the meniscus volume, S_{lid} is the lid perimeter, R_{im} is the tear-meniscus radius, q_{laci} is the volumetric lacrimal flow rate entering the meniscus from the conjunctival sac where $q_{lacu} = 0.8q_{lac}$ and $q_{lacl} = 0.2q_{lac}$, $q_{di} = q_m(1 - R_0/R_{im})$ is the volumetric tear-

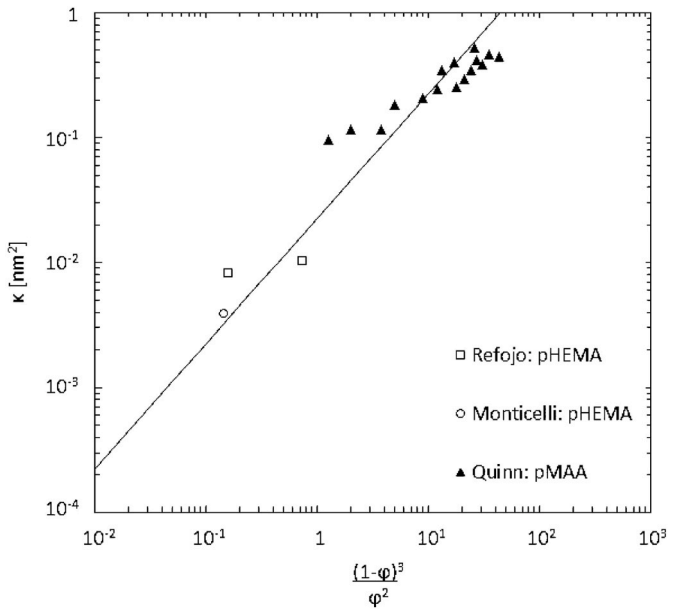

Fig. 9. Hydrodynamic permeability, K, as a function of polymer content expressed as $(1-\varphi)^3/\varphi^2$ for hydrogels similar to 70-wt% hydroxyethylmethacrylate (HEMA)/30-wt% methacrylic acid (MAA): Refojo (1965) (□); Quinn and Grodzinsky (1993) (▲); Monticelli et al. (2005) (○). With $a_f = 2$ nm, the best-fit unity-slope straight line on log-log scales gives a hydrodynamic tortuosity of $\tau_H = 4.7$. Reprinted with permission from Liu et al. (2013). Copyright (2013) American Chemical Society.

Table 3
Physical constants.

PARAMETER	SYMBOL (UNIT)	VALUE
Lid margin perimeter	S_{lid} (mm)	30[a]
Maximum drainage rate	q_m $(\mu L/\min)$	1.0[b]
Minimum drainage radius	R_0 (μm)	120[b]
Bulbar conjunctival area uncovered by eyelid	A_{cj} (cm^2)	1.05[a]
Lens area uncovered by eyelid	A_{lens} (cm^2)	1.54[c]
Corneal area uncovered by eyelid	A_{cn} (cm^2)	1.05[a]
Lens water concentration	$c_{w,lens}$ (mol/cm^3)	0.02[c]
Lens hydraulic water permeability	K (μm^2)	9.7×10^{-9}[d]
Lens thickness	h_{lens} (μm)	60–200
Interblink period	t_{ib} (s)	5–30
Lens salt diffusivity	D_s (cm^2/s)	$0\sim6\times10^{-6}$
Salt partition coefficient	k_s	0–1
Secreted tear salt concentration	c_{blink} $(mOsM)$	150[a]
Salt diffusivity in water	D_∞ (cm^2/s)	2.25×10^{-5}[e]
Gas constant	R $(J/(mol*K))$	8.3145
Temperature	T (K)	310
Reflection coefficient of salt	σ_{cn}	0.79[f]
Corneal epithelium membrane salt permeability	ω_{cn} (cm/s)	7.37×10^{-11}[f]
Water volume fraction	φ_w	0.38[g]
Length from lens center to meniscus	λ (mm/s)	5.5

[a] Obtained from Cerretani and Radke (2014).
[b] Obtained from Zhu and Chauhan (2005).
[c] See Main Text.
[d] Obtained from Monticelli et al. (2005).
[e] Obtained from Pratt and Wakeham (1977).
[f] Obtained from Leung et al. (2011).
[g] Determined from Hoch et al. (2003) and Guan et al. (2011).

drainage rate based on Cerretani and Radke (2014) of upper $(i=u)$ or lower $(i=l)$ puncta, q_m is the maximum drainage rate, and R_0 is the meniscus radius when drainage ceases. q_{di} changes transiently due to dependence on the shrinking menisci radii and ranges between 0 and 1.00 μL/min based on q_m and R_0 determined by Cerretani and Radke (2014) to match the results of Zhu and Chauhan (2005). As previously stated, the maximum tear-drainage rate (i.e., $q_d = q_{du} + q_{dl}$) is 2.00 μL/min. Calculated q_d values fall within the range of tear-turnover rates tabulated (i.e., 0.12–1.47 μL/min) by Tomlinson and Khanal (2005). $q_{e,im}$ is the set volumetric evaporation rate of upper or lower menisci and is determined by multiplying the volumetric evaporation flux, $\widetilde{J}_{w,e}$, with the cross-sectional area of upper or lower meniscus ($A_{im} = \pi R_{im} S_{lid}/2$). Additional detail regarding this mass balance is provided in Appendix B of Cerretani and Radke (2014).

Salt conservation for each tear meniscus reads

$$\frac{d(c_{im}V_{im})}{dt} = c_{si}q_{laci} - c_{im}q_{di} \qquad i = u, l \tag{4}$$

where c_{si} is the salt concentration of the conjunctival sac and c_{im} is the salt concentration of the meniscus. c_{im} depends on the tear-film salt concentration from the well-mixed blink period and the lacrimal gland salt concentrations. Although the upper and lower menisci osmolarities are calculated separately, the two menisci osmolarities are approximately the same due to their large tear volumes.

4.2.2. Pre-conjunctival tear-film balances

Aqueous conservation in the palpebral aperture not covered by the contact lens (i.e., the PrCjTF) is similar to that of the pre-corneal tear film (Cerretani and Radke, 2014; You et al., 2013). However, water is gained only from osmotic-driven flow through the bulbar conjunctiva instead of from both the bulbar conjunctiva and the cornea. Water conservation for this region is written as

$$\frac{dV_{PrCj}}{dt} = -q_{e,PrCj} + \alpha q_{cj} \tag{5}$$

where V_{PrCj} is the volume of water in the PrCjTF, $q_{e,PrCj} = A_{cj}\widetilde{J}_{w,e}$ is the volumetric evaporation rate of tear for the PrCjTF, $q_{cj} = A_{cj}\widetilde{J}_{w,cj}$ is the volumetric flow rate of water from the bulbar conjunctiva into the PrCjTF, A_{cj} is the cross-sectional area of the bulbar conjunctiva that is uncovered by the eyelids, $\widetilde{J}_{w,cj}$ is the volumetric water flux from the bulbar conjunctiva, and α is the fraction of bulbar conjunctiva not covered by the contact lens and the eyelids. Detailed information to determine α is provided in Appendix A. Calculation of $\widetilde{J}_{w,cj}$ is outlined in Appendix B of Cerretani and Radke (2014).

The bulbar conjunctiva secretes ions into the PrCjTF (Dartt, 2002) but the rate is not expected to be large (Cerretani and Radke, 2014; Leung et al., 2011). Thus, salt conservation for the PrCjTF is written as

$$\frac{d\left(c_{PrCj}V_{PrCj}\right)}{dt} = 0 \tag{6}$$

where c_{PrCj} is the transient salt concentration in the PrCjTF.

4.2.3. Pre-lens tear-film balances

New PrLTF and PoLTF compartments unique to SCL wear are added to the previous Cerretani-Radke model (Cerretani and Radke, 2014) to determine the osmolarities of the two tear films. Because SCLs are permeable to both salt and water, PrLTF osmolarity depends on both tear evaporation and transport of salt and water across the contact lens. Water conservation for the PrLTF is described by

$$\frac{dV_{PrL}}{dt} = -q_{e,PrL} + q_{lens} \tag{7}$$

where V_{PrL} is the volume of water in the PrLTF, $q_{e,PrL} = A_{lens}\widetilde{J}_{w,e}$ is the

volumetric evaporation rate of tear for the PrLTF, $q_{lens} = A_{lens}\widetilde{J}_{w,lens}$ is the volumetric water transport rate across the lens, A_{lens} is the cross-sectional area of the lens exposed to the environment, and $\widetilde{J}_{w,lens}$ is the volumetric water flux across the lens. Details regarding $\widetilde{J}_{w,lens}$ are provided in Section 4.2.4.

Salt conservation in the PrLTF is mathematically represented as

$$\frac{d(c_{PrL}V_{PrL})}{dt} = A_{lens}J_{s,lens} \tag{8}$$

where $J_{s,lens}$ is the molar salt flux at the anterior surface of the lens directed from the PoLTF to the PrLTF. Because the difference in salt concentration between the PrLTF and PoLTF can be either positive or negative, $J_{s,lens}$ similarly may be positive or negative. Details regarding $J_{s,lens}$ are provided in Section 4.2.4.

4.2.4. Soft-contact-lens balances

Volumetric water flux across the lens follows a modified Darcy law and is given by

$$\widetilde{J}_{w,lens} = v_w = \frac{2KRT}{\mu_w}\frac{(c_{PrL} - c_{PoL})}{h_{lens}} \tag{9}$$

where R is the ideal gas constant, T is the temperature of the lens, c_{PrL} is the PrLTF salt concentration, and c_{PoL} is the PoLTF salt concentration. Detailed derivation is provided in Appendix B. $\widetilde{J}_{w,lens}$ is determined from the osmotic salt-concentration difference between PoLTF and PrLTF and can be positive or negative depending on that difference.

Water-flow-driven salt convection and salt diffusion determine the salt flux at the PrLTF and PoLTF lens interfaces. The transient salt concentration profile across the lens is determined from the following partial differential equation

$$\frac{\partial c_{lens}}{\partial t} + \widetilde{J}_{w,lens}\frac{\partial c_{lens}}{\partial z} = D_s\frac{\partial^2 c_{lens}}{\partial z^2} \tag{10}$$

where c_{lens} is the salt concentration within the lens per unit lens volume and z is the spatial location within the lens from the posterior ($z = 0$) to the anterior ($z = h_{lens}$). Equation (10) is solved numerically with finite differences and boundary conditions: $c_{lens}(0) = k_s c_{PoL}$ and $c_{lens}(h_{lens}) = k_s c_{PrL}$. Transient solution to Equation (10) is nested within each time step of the numerical solution of the ordinary differential equation tear-compartment balances. Therefore, the iteration time step used for the lens salt balance is 0.001 s and is an order of magnitude smaller than the time step used to solve the compartment mass balances. Convergence for the nested numerical evaluation of Equation (10) is achieved for each of the time steps used for the compartment mass balances.

Once the lens-salt transient concentration profile is established at each compartmental time step, molar salt fluxes at the PrLTF and PoLTF lens interfaces are calculated by the expression

$$J_{s,lens} = \widetilde{J}_{w,lens}c_{lens} - D_s\frac{\partial c_{lens}}{\partial z} \qquad z = 0,\ h_{lens} \tag{11}$$

Lens salt flux is evaluated at the lens anterior surface, $z = h_{lens}$, and at the lens posterior surface, $z = 0$, and is used in the PrLTF and PoLTF compartment balances of Equations (8) and (13) (to follow), respectively. Further details regarding lens-salt transport are outlined in Appendix C.

4.2.5. Post-lens tear-film balances

In addition to water flow from/to the lens, water also flows from the cornea and the bulbar conjunctiva into the PoLTF. Therefore, water conservation in the PoLTF is given by the relation

$$\frac{dV_{PoL}}{dt} = (1-\alpha)q_{cj} + q_{cn} - q_{lens} \tag{12}$$

where V_{PoL} is the volume of water in PoLTF, $q_{cn} = A_{cn}\widetilde{J}_{w,cn}$ is the volumetric flow rate of water from the cornea into the PoLTF, A_{cn} is the cross-sectional area of the cornea not covered by the eyelids, and $\widetilde{J}_{w,cn}$ is the volumetric water-flux supply from the cornea. Details regarding $\widetilde{J}_{w,cn}$ are presented in Appendix B of Cerretani and Radke (2014). Again, q_{lens} is the volumetric water-transport rate across the lens obtained from Equation (9).

Similar to lens water flow, there is a salt flux into/out of the PoLTF across the lens during the interblink period. In addition, salt transports from the cornea into the PoLTF (Leung et al., 2011). Salt transport across the bulbar conjunctiva is ignored, as previously discussed. Salt conservation in the PoLTF is, therefore, represented as

$$\frac{d(c_{PoL}V_{PoL})}{dt} = -A_{lens}J_{s,lens} + \left[(1-\sigma_{cn})\widetilde{J}_{w,cn} < c_{cn} > -\omega_{cn}RT\Delta c_{cn}\right]A_{cn} \tag{13}$$

where the bracketed terms represent the Kedem-Katchalsky membrane equation for salt transport across the cornea (Kedem and Katchalsky, 1958) and $J_{s,lens}$ is the molar salt flux through the SCL from Equation (11). σ_{cn} is the corneal-epithelium reflection coefficient of salt, $< c_{cn} >$ is the arithmetic average salt concentration in the corneal epithelial layer, ω_{cn} is the corneal epithelium membrane permeability to salt, and Δc_{cn} is the salt-concentration difference between the PoLTF and the corneal epithelium. Details and constants of the Kedem-Katchalsky equation can be found in Leung et al. (2011). σ_{cn} and ω_{cn} are those of sodium or chloride; the corneal epithelial salt concentration is set as 150 mOsM.

4.3. Eyelid closure

At the end of the interblink period, the eyelid takes approximately 0.2 s to close (Cerretani and Radke, 2014; Fatt and Weissman, 1992). During this phase, salt and water in the menisci, conjunctival sacs, PrLTF, PrCjTF, and a fraction of the PoLTF all mix together. The mixed concentration, c_{bulk}, is the same for all compartments, except the PoLTF, for the next interblink period. Salt and water balances during the mixing process are given by

$$c_{bulk}V_{total} = c_{PrL}V_{PrL} + c_{PrCj}V_{PrCj} + c_{um}V_{um} + c_{lm}V_{lm} + c_{su}V_{su} + c_{sl}V_{sl} + c_{blink}V_{blink} + \beta c_{PoL}V_{PoL} \tag{14}$$

and

$$V_{total} = V_{PrL} + V_{PrCj} + V_{um} + V_{lm} + V_{su} + V_{sl} + V_{blink} + \beta V_{PoL} \tag{15}$$

respectively. V_{blink} and c_{blink} are tear volume and salt concentration produced by the lacrimal glands during the blink phase, respectively. Lacrimal-production details are provided in Appendix D. V_{total} is the total volume of the mixed-tear compartments during the blink phase, c_{bulk} is the concentration of the mixed-tear compartments during the blink phase, V_{um} is the upper-meniscus tear volume, c_{um} is the upper-meniscus salt concentration, V_{lm} is the lower-meniscus tear volume, V_{su} is the upper conjunctival-sac tear volume, c_{su} is the upper conjunctival-sac salt concentration, V_{sl} is the lower conjunctival-sac tear volume, and c_{sl} is the lower conjunctival-sac salt concentration. Since the upper and lower conjunctival-sac salt concentrations correspond to profiles from the end of the fornix to the upper and lower menisci, respectively, the concentration profile in each fornix is averaged for evaluating Equation (14). Mixing of the conjunctival sacs and other tear compartments is due to the motion of the lids and the eye. Cerretani and Radke (2014) found only small differences in compartment osmolarities for no mixing and well mixing of the conjunctival sacs. Due to the very short blink time, bulbar and conjunctival tear production during the blink phase are negligible and, thus, are ignored. β is the fraction of PoLTF that mixes with the total tear film during each blink cycle. V_{PoL} at the beginning of deposition phase is set so that the PoLTF thickness is 2 μm at the start of the deposition phase. Accordingly, β is determined so

that tear entering the PoLTF from mixing is 1% of the set PoLTF deposition volume (McNamara et al., 1999).

5. Results and discussion

For the small values of hydraulic permeabilities, K, for commercial SCLs in Fig. 9, water flow through the lens has minimal effect on all tear-compartment osmolarities. As discussed in Appendix E, comparison between perched and non-perched tear films also reveals no difference in tear osmolarity for all tear compartments. Further, salt diffusion between PrLTF and PrCjTF is also negligible since the salt-concentration difference between the PrLTF and PrCjTF is smaller than that between the PrLTF and the tear menisci. Therefore, we assume that the PrLTF and the PrCjTF are perched and isolated from the menisci, and that there is no transport between the PrLTF and the PrCjTF. The following subsections present results of tear-compartment osmolarities for various lens salt-transport properties and tear-production and tear-evaporation rates. In Sections 5.1 and 5.2, we analyze the impact of SCL wear on PoLTF salinity in normal and dry eyes, respectively. In Section 5.3, we assess the individual effect of tear evaporation rate and tear production rate on PoLTF osmolarity. Effect of lens properties on PoLTF osmolarity is explored in Section 5.4 and the effect of interblink duration on PoLTF osmolarity is investigated in Section 5.5. In all subsections, we focus on what circumstances SCLs might protect the cornea against hyperosmolarity.

5.1. Effect of lens-salt diffusivity for normal eyes

Fig. 10 portrays the effect of the lens-salt diffusion coefficient, D_s, on tear-compartment osmolarities as a function of time for normal eyes while keeping other variables constant. Evaporation and lacrimal production rates used for this analysis are provided in the first row of Table 2. The selected D_s values in Fig. 10 fall within the range of commercially available SCLs today (Guan et al., 2011; Mann et al., 2019) (see also Fig. 7). Repeated "shark-fin" patterns represent separate blink cycles in periodic-steady state (i.e., osmolarity patterns repeat every blink). All compartments experience periodic increases in osmolarity but menisci and PoLTF cycle changes are small and thus not apparent on the ordinate scale chosen of Fig. 10. As expected, the largest fluctuations in osmolarity are seen in the PrLTF and PrCjTF because of tear evaporation (Fig. 10, red and black lines, respectively).

The most important finding in Fig. 10 is that by decreasing D_s, the PoLTF is immunized against hyperosmolarity as shown by the blue line in Fig. 10a. In fact, with low enough D_s, PoLTF osmolarity is even lower than that in the tear meniscus. Conversely, large D_s values result in PoLTF osmolarities similar to those of the PrLTF and PrCjTF as shown in Fig. 10c. Moreover, the lower is the D_s value, the more drastic is the increase in PrLTF salt concentration because less salt transfers across the lens. PrLTF osmolarity is higher than that of PrCjTF during the interblink period because of the thinner deposited tear film over the SCL (see Section 2.2) than over the bulbar conjunctiva, which makes PrLTF more susceptible to evaporation-driven salt concentration increase compared to the PrCjTF. Due to the relative large volume and small exposed

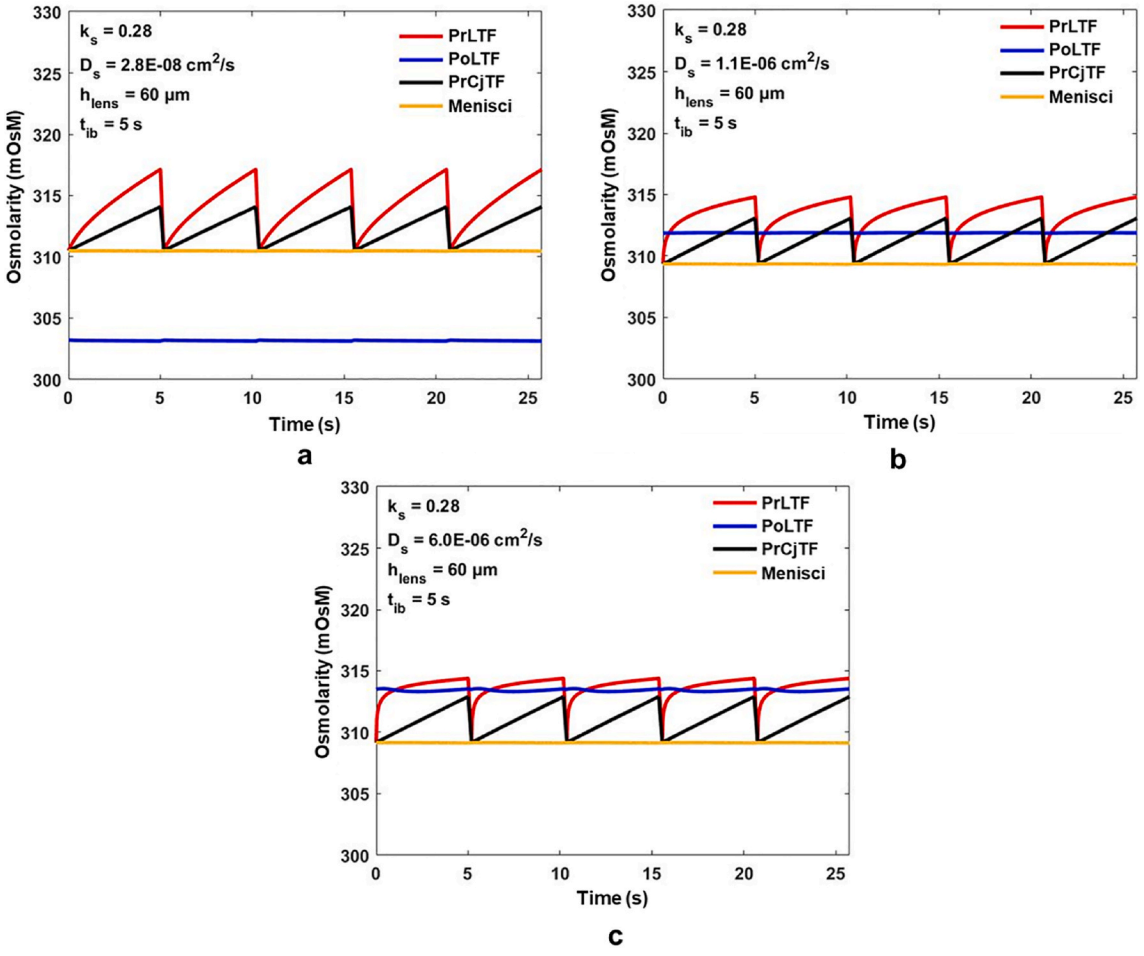

Fig. 10. Periodic-steady tear osmolarity of PrLTF, PoLTF, PrCjTF, and tear menisci for normal eyes. (a) low D_s ($= 2.8 \times 10^{-8} cm^2/s$), (b) medium D_s ($= 1.1 \times 10^{-6} cm^2/s$), and (c) high D_s ($= 6.0 \times 10^{-6} cm^2/s$). Interblink period is 5 s. Tear evaporation rate is that of normal no-lens wear from Table 2. All parameters are constant except salt diffusivity, D_s.

surface area to environmental evaporation, both upper and lower meniscus osmolarity change is insignificant during the interblink period. During every blink period, all tear-compartment osmolarities converge to the same well-mixed value except for the PoLTF, as illustrated in Fig. 3. This is reflected at the beginning of each interblink cycle of Fig. 10. Different osmolarity of the PoLTF than the tear compartments at the beginning of each interblink cycle also indicates that the relatively small (1–2%) of PoLTF tear exchange upon every blink is not a significant mechanism to prevent hyperosmolarity in the PoLTF during SCL wear.

At the beginning of each interblink period for SCLs with higher D_s (i.e., Fig. 10b–c), the PrLTF osmolarity is lower than that of the PoLTF. In these cases, salt travels from the PoLTF to the PrLTF until, at some later time point in the blink cycle, the increased PrLTF osmolarity, due mainly to evaporation, becomes higher than that of the PoLTF. During this initial phase of the interblink period, water transport, albeit small, occurs from the PrLTF to the PoLTF. Thus, PoLTF osmolarity also decreases during this initial time interval. This finding is qualitatively visible in Fig. 10c but is not as apparent in Fig. 10b because the PoLTF and PrLTF osmolarity difference at the beginning of the interblink period is smaller than that in Fig. 10c. Once the PrLTF osmolarity becomes higher than that of the PoLTF, salt transports from the PrLTF to PoLTF and water flows from the PoLTF to PrLTF. For Fig. 10a, where the PoLTF osmolarity is always lower than the PrLTF, salt always travels from the PrLTF to PoLTF while the water transports in the opposite direction from the PoLTF to the PrLTF within every blink cycle.

5.2. Effect of lens-salt diffusivity for dry eyes

To represent dry-eye conditions, an increased evaporation rate, q_e, and a reduced production rate, q_{lac}, compared to those in normal eyes are selected for analysis (see second row, Table 2). Fig. 11 displays the influence of D_s on tear-compartment osmolarities for dry-eye conditions. All remaining variables are constant and identical to those in the normal-eye analysis of Fig. 10. Due to the higher evaporation and lower lacrimal production rates, osmolarities are elevated in Fig. 11 for all compartments compared to those of normal eyes. Although similar patterns are observed compared to those for normal eyes (i.e., PrCjTF osmolarity is lower than that of the PrLTF, and menisci osmolarity is lower than those for both PrCjTF and PrLTF) osmolarity fluctuations are more sensitive to D_s with dry eye than they are with normal eyes. With the low-diffusivity SCL in Fig. 11a, the osmolarity in the PoLTF is lower than that of the menisci of a dry eye without lens wear reported by Tomlinson et al. (2006) and displayed in Fig. 1. PoLTF osmolarity in Fig. 11a is approximately the same as that of the menisci of normal eye with lens wear (Fig. 10, yellow lines). This observation reinforces the potential for a SCL to protect the corneal surface from hyperosmolarity, especially for dry eyes. However, such protection gradually deteriorates with higher D_s, as shown in Fig. 11b and c.

Although decreasing D_s decreases the PoLTF osmolarity, the dry-eye analysis discloses that decreasing D_s increases the menisci, PrLTF, and PrCjTF osmolarities, which is similar to the observation from the normal-eye analysis in Section 5.1. Again, the inverse effect of D_s on menisci, PrLTF, and PrCjTF osmolarities due to less salt transported to

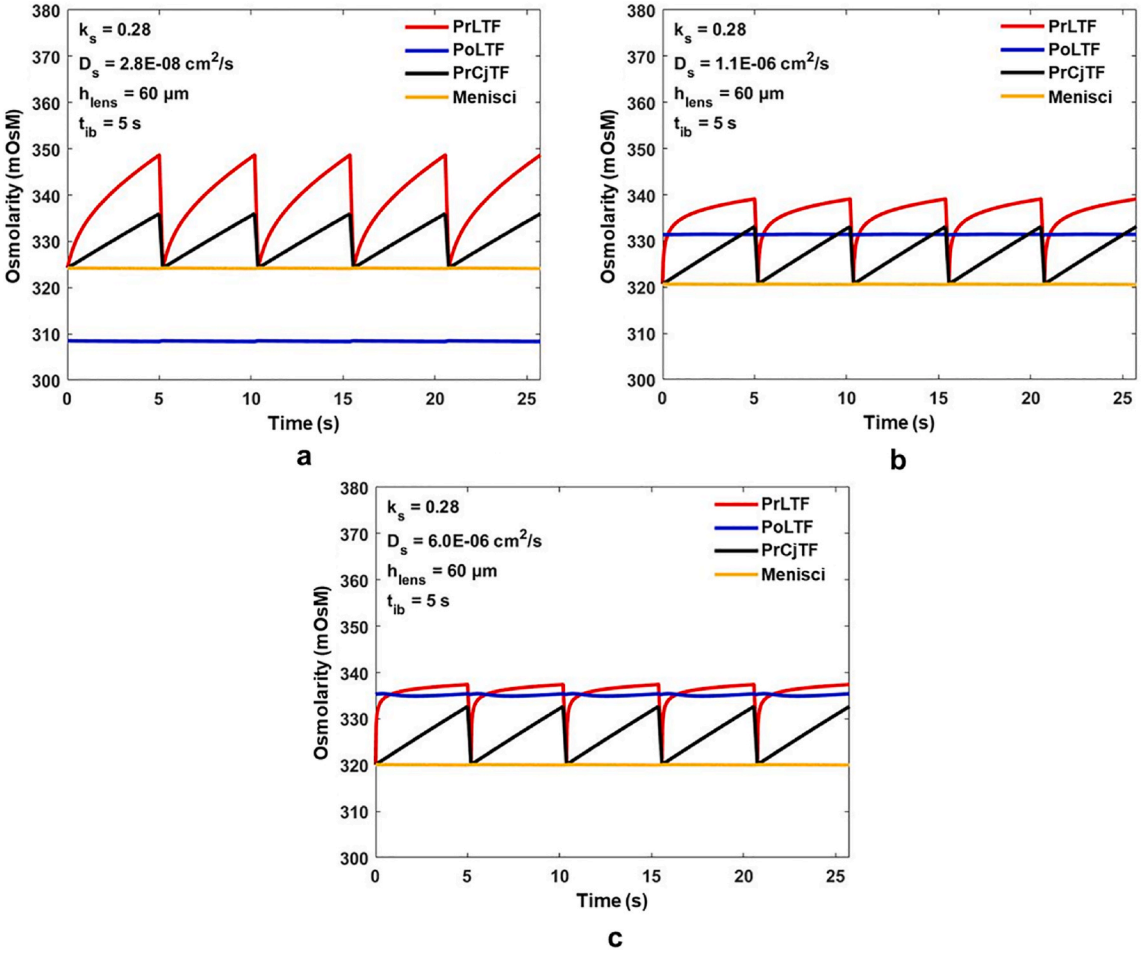

Fig. 11. Periodic-steady tear osmolarity of PrLTF, PoLTF, PrCjTF, and tear menisci for dry eye. (a) low D_s ($= 2.8 \times 10^{-8} cm^2/s$), (b) medium D_s ($= 1.1 \times 10^{-6} cm^2/s$), and (c) high D_s ($= 6.0 \times 10^{-6} cm^2/s$). Tear evaporation and production rates are those of dry eye from Table 2. Other than tear evaporation and production rates, all parameters in Fig. 11 are identical to those in Fig. 10. Interblink period is 5 s.

the PoLTF during the interblink period is more sensitive with smaller D_s in dry eye compared to that in normal eye.

5.3. Effects of tear-evaporation and lacrimal-production rates

Guillon and Maissa (2008) documented a 40–50% increase in ocular-surface evaporation rate during SCL wear. Since their study did not separate normal and dry-eye subjects, Fig. 12 assesses how an increase in evaporation rate by 50% on a normal eye affects the osmolarities of the tear compartments during SCL wear. Tear-evaporation and lacrimal-production rates used are documented in the third row of Table 2. Remaining parameters are the same as those for Fig. 10b.

In Fig. 12, the increase in evaporation rate by 50% of the normal eye for SCL wear while keeping lacrimal-production rate constant increases osmolarity in all tear compartments by ~5 mOsM. Thus, ineffective evaporation retardation by the tear lipid layer of the PrLTF during SCL wear (Cedarstaff and Tomlinson, 1983) is important to tear-compartment osmolarities. Since the effect of SCL wear on tear-production rate is unknown, we also investigated the effect of increased lacrimal-production rate while maintaining a constant evaporation rate. Evaporation rate of a normal eye (first row, second column of Table 2) and lacrimal-production rate of a dry eye (second row, first column of Table 2) with medium lens D_s result in a PoLTF osmolarity that is ~3 mOsM greater than that of a normal eye with medium lens D_s wear previously shown in Fig. 10b. These results accentuate the importance of tear production and evaporation on tear osmolarity during SCL wear.

5.4. Effect of lens properties on PoLTF salinity

To clarify further the effect of lens properties (i.e., D_s, k_s, and h_{lens}) on PoLTF salinity, a series of calculations varying individual properties was conducted and findings are summarized in Figs. 13–15. Fig. 13 highlights the relationship between the time-averaged PoLTF osmolarity and D_s for normal eyes with a blink interval of $t_{ib} = 5$ s. As before, the D_s range chosen in Fig. 13 lies within the range of what is available with commercially available SCLs today (Guan et al., 2011; Mann et al., 2019). At low D_s, PoLTF osmolarity declines sharply because lens resistance to salt transport increases drastically. The shaded region in Fig. 13 accentuates the corresponding osmolarities in the tear menisci where in-vivo salt concentrations are measured. When the lens-salt

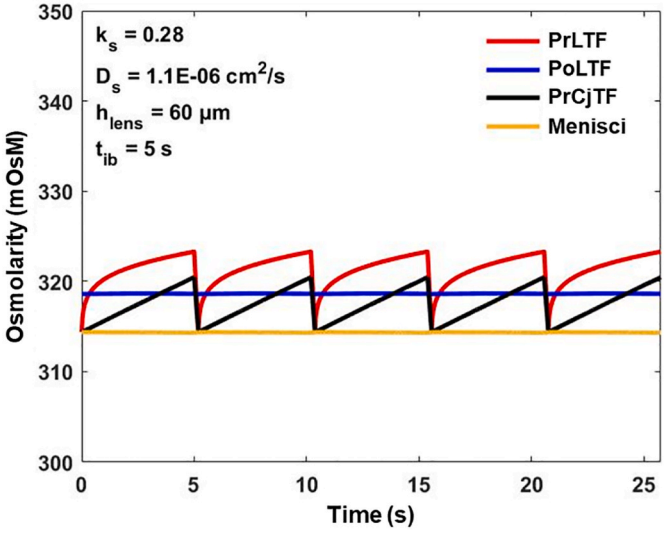

Fig. 12. Periodic-steady tear osmolarity of PrLTF, PoLTF, PrCjTF, and tear menisci for normal eye with lens wear with higher evaporation rate. Tear evaporation rate is that of normal lens-wear based on measurements of Guillon and Maissa (2008) listed in Table 2. Interblink period is 5 s.

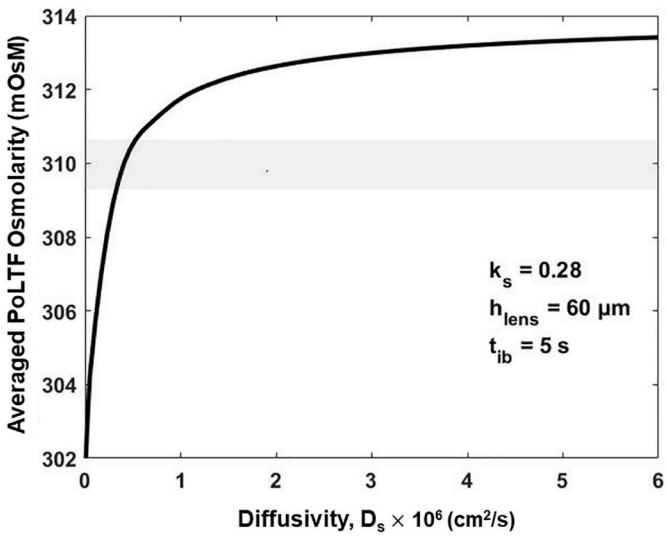

Fig. 13. Time-averaged PoLTF tear osmolarity as a function of lens-salt diffusivity for normal eyes. Shaded region corresponds to menisci salt concentration for normal eyes.

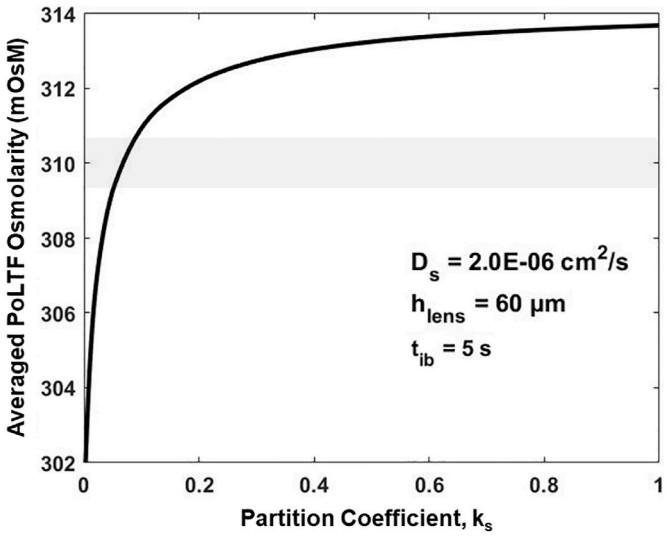

Fig. 14. Time-averaged PoLTF tear osmolarity as a function of lens-salt partition coefficient for normal eyes. Shaded region corresponds to menisci salt concentration for normal eyes.

diffusivity, D_s, falls below about $5 \times 10^{-7} cm^2/s$ for normal (Fig. 13) and dry-eye (not shown) SCL wear, the PoLTF osmolarity falls below that in the tear menisci. Lenses with D_s below this value can provide protection against corneal hyperosmolarity.

Fig. 14 portrays the effect of salt partition coefficient, k_s, on time-average PoLTF osmolarity keeping all other parameters constant and $t_{ib} = 5$ s. Again, the shaded region encompasses osmolarities in the tear menisci. Both D_s and k_s have significant effects on lowering PoLTF osmolarity when their values are low. When their values are high, sensitivity to their values diminishes. Although low k_s values reduce PoLTF osmolarity, the range of k_s currently available for SCLs is 0.15–0.70 (Guan et al., 2011). Within this range, k_s affects PoLTF osmolarity by ~2 mOsM. Since D_s and k_s act independently in transient lens-salt diffusion rather than as the product of the two (i.e., $D_s k_s$ or salt permeability) focus should be more on reducing D_s to lower PoLTF osmolarity for SCL wear.

Fig. 15 graphs the effect of lens thickness, h_{lens}, on time-averaged

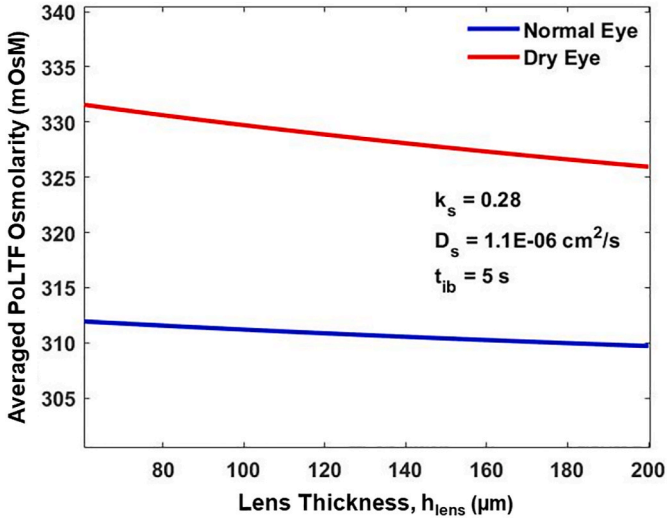

Fig. 15. Time-averaged PoLTF tear osmolarity as a function of lens thickness for normal and dry eyes.

PoLTF osmolarity for normal and dry eyes. Thicker lenses result in lower PoLTF osmolarity as expected since the lens thickness affects the salt transport resistance. Similar to the effect of D_s, PoLTF osmolarity is more sensitive to h_{lens} in dry eye than it is in normal eye. Overall, however, the influence of h_{lens} on PoLTF osmolarity is not strong within the limited range of SCL thickness for comfortable wear, partly because during each periodic interblink, salt diffusion through the lens does not reach pseudo steady state. Accordingly, salinity fluctuations in the PrLTF do not significantly penetrate through the lens. To minimize PoLTF hyperosmolarity, ideal lens designs should primarily minimize D_s.

5.5. Effect of interblink period on PoLTF salinity

All above analyses were conducted assuming a normal blink pattern of a 5-s interblink. Because a longer interblink period, t_{ib}, allows more time for tear to evaporate, PoLTF osmolarity clearly depends on how frequent SCL wearers blink their eyes. Fig. 16 shows the effect of t_{ib} on the time-averaged PoLTF osmolarity. As expected, PoLTF osmolarity increases with longer t_{ib}. This result may help explain why lens wearers feel discomfort when they blink infrequently and feel the urge to blink

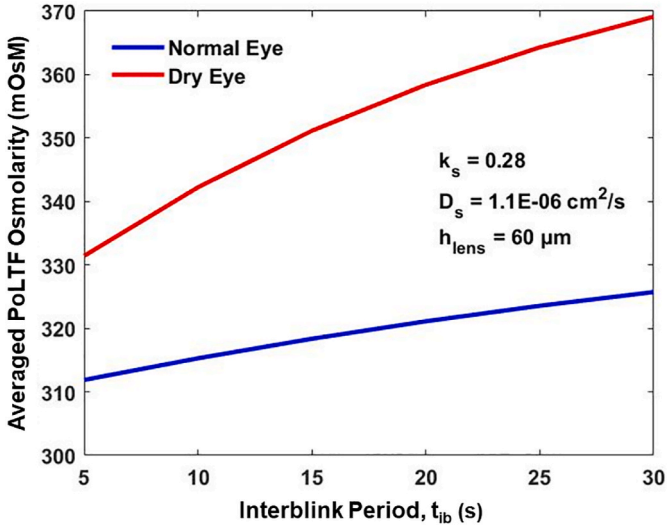

Fig. 16. Time-averaged PoLTF tear osmolarity as a function of interblink period for normal and dry eyes.

when they do not blink frequently enough. Similar to lens properties, PoLTF osmolarity is more sensitive to t_{ib} for dry eye than for normal eye.

5.6. Comparison between SCL wear and no-lens wear

To evaluate how lens-wear osmolarities for various tear compartments compare to those for no-lens wear, results from normal-eye lens-wear (Fig. 10a) and normal-eye no-lens-wear (Fig. 1) are plotted together in Fig. 17 for ease of comparison. All tear-evaporation and tear-production parameters are kept the same. Menisci osmolarities of no-lens wear are slightly lower than those of the menisci osmolarities during SCL wear (by ~ 2 mOsM). This observation is consistent with clinical studies that measured meniscus osmolarity with and without lens wear (Golebiowski et al., 2017; İskeleli et al., 2002; Kojima et al., 2011; Martin, 1987; Sarac et al., 2012; Stahl et al., 2009) and is explainable by the fact that the menisci volumes with lens wear are slightly larger than those for no-lens wear because of the thinner tear film deposited with lens wear than without lens wear. However, normal-eye lens-wear menisci osmolarities do not reach the elevated menisci osmolarities of those with dry-eye no-lens wear. This observation potentially explains why elevated meniscus osmolarity during lens wear does not correlate with lens-wear discomfort (Stahl et al., 2009). Fig. 17 also demonstrates that the PrLTF osmolarity rises significantly higher than that of the PrCTF during no-lens wear. This too is due to the thinner deposited PrLTF than that of the PrCTF.

Comparison between PrCTF osmolarity for normal and dry eyes with no-lens wear (Fig. 1) to that of PoLTF osmolarity for lens-wear normal (Fig. 10) and dry eyes (Fig. 11) shows that lens wear can increase or decrease significantly the osmolarity of the tear interfacing the cornea. Although a direct correlation of PoLTF osmolarity to ocular safety and comfort is not available to date due to the limited understanding of PoLTF osmolarity, positive correlation between no-lens-wear dry-eye symptoms and osmolarity (Farris, 1986; Farris et al, 1981, 1983; Gilbard, 1994; Gilbard et al., 1978; Mathers et al., 1996; Mishima et al., 1971; Ogasawara et al., 1996; Tomlinson et al., 2006) suggests that PoLTF hyperosmolarity could positively correlate with lens-wear discomfort. Although osmolarity for PrCTF during an interblink period is significantly higher than that of PoLTF in Fig. 17, higher D_s can result in peak osmolarities in the PrCTF higher than those for the PoLTF while the time-averaged osmolarities in the PoLTF are higher than those of PrCTF (not shown). The significance of higher time-averaged osmolarity

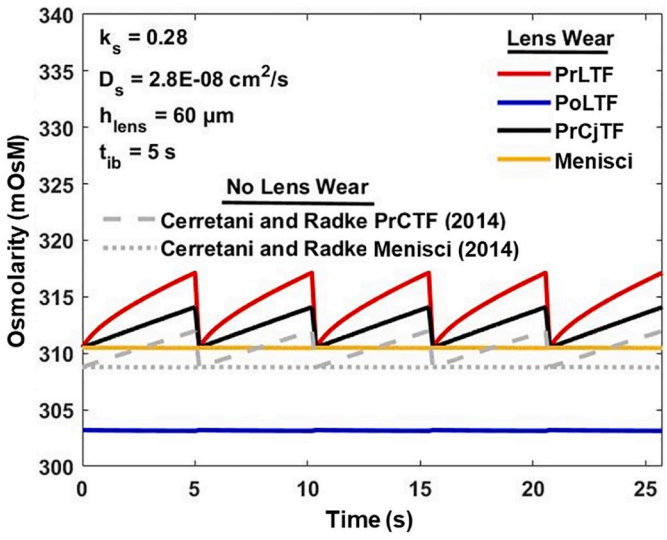

Fig. 17. Periodic-steady tear osmolarity during lens wear compared to no-lens wear. Tear evaporation and production rates are those of normal no-lens wear from Table 2. All lens properties are identical to those of Fig. 10a. No-lens wear data are those of normal eyes from Fig. 1. Interblink period is 5 s.

versus the peak osmolarity observed at the end of each interblink on lens-wear discomfort remains unknown. In either case, tear-meniscus osmolarity is not a good representation of PrCTF and PoLTF osmolarities, which are those in direct contact with the corneal epithelium during no-lens wear and lens wear, respectively.

6. Conclusions and future directions

For the first time, our proposed physiological-based mathematical model interrogates the PoLTF osmolarity during SCL wear and demonstrates the importance of lens-material properties, PrLTF thickness, and lipid-layer quality on PoLTF osmolarity. Our time-periodic tear-compartment continuum model predicts that SCL wear can protect the cornea from hyperosmolarity even when the PrLTF is hyperosmolar. To produce a low PoLTF osmolarity with SCL wear, both D_s and k_s should be reduced while increasing h_{lens}. However, practical material limitations constrain h_{lens} and k_s. Further, maximizing oxygen delivery to the ocular surface to avoid corneal hypoxia relies on minimizing the h_{lens} (Kim et al., 2020; Leung et al., 2011; Takatori and Radke, 2012). Thus, SCLs designed to avoid corneal hyperosmolarity should focus on lowering lens D_s. Too low a salt diffusivity, however, can adhere the lens to the ocular surface (Cerretani et al., 2012; Nicolson et al., 1999). To prevent lens adherence, Nicolson et al. (1999) suggest a minimum D_sk_s threshold of $2\,x10^{-7}cm^2/s$. The actual minimum threshold value may be lower based on more recent D_sk_s measurements of commercial SCLs (Guan et al., 2011; Mann et al., 2019). Nevertheless, the threshold of Nicolson et al. (1999) is a helpful guideline.

The significant difference between the PoLTF osmolarity and the tear menisci during lens wear emphasizes the need to investigate the correlation between lens-wear discomfort and PoLTF osmolarity. As osmolarity has been shown to correlate with dry-eye symptoms (e.g., irritation, stinging, burning, prickling, and cooling) during no-lens wear (Liu et al., 2009), it is likely that the PoLTF osmolarity correlates with lens-wear discomfort that has the same etiology as dry eyes but not other forms of discomfort induced by lid-wiper epitheliopathy, blurry vision, lens edge, SCL surface dehydration, or other forms of lens awareness. To answer this important clinical question, a method to measure PoLTF osmolarity in vivo is requisite. Recent developments in sensor technology with contact lenses hold promise (Jones et al., 2021; Kim et al., 2017). Chiou (2019) developed a prototype contact lens with electronics to measure tear osmolarity continuously. However, no peer-reviewed manuscript is available to date for detailed information. Also, multiple groups are actively investigating contact lenses with fluorescent dyes embedded to measure ion concentrations (Badugu et al., 2018; Yetisen et al., 2020). For ion-specific fluorophores to determine the PoLTF concentration accurately, additional investigation is needed on how well fluorophores bind only to the targeted ions clinically. Finally, sensor-embedded contact lenses must ensure that the tagged lens material and/or sensor embedments are designed compatible with conventional SCLs. Otherwise, the prototype lenses may not mimic those of commercially available SCLs today.

PoLTF osmolarity is near constant throughout the interblink period. Conversely, PrCTF osmolarity without lens wear increases rapidly during the interblink period. Depending on the lens material, PoLTF time-averaged osmolarity can be higher than that of the PrCTF with no-lens wear but not higher than the peak osmolarity. In such a situation, the question arises whether lens wear or no-lens wear results in more osmolarity-driven discomfort. It is possible that protection against high peak osmolarity of the PrCTF with lens wear is the reason why lens wearers, compared with no-lens wear, have longer maximum interblink intervals during a stress test (Zhang et al., 2017). The effect of time-averaged osmolarity and interblink peak osmolarity on ocular discomfort requires investigation. Importantly, SCL wearers should put conscious effort into blinking more frequently because longer interblink times increase PoLTF osmolarity significantly.

Our tear-dynamics osmolarity analyses on normal and dry eyes reveal that tear-production and tear-evaporation rates have a significant effect on the tear osmolarity during SCL wear. Therefore, robust meibomian-gland lipid expression and lacrimal-tear production, common metrics for assessing evaporative and aqueous-deficient dry eyes, should be considered in optimal SCL fitting. Our proposed tear-dynamics SCL model also shows that lens properties have greater effect on tear osmolarity for dry eyes than for normal eyes. With lower D_s values, SCLs can protect against hyperosmolarity for normal and especially for individuals suffering from dry eyes. Further studies are needed to determine the optimal lens D_s, k_s, and h_{lens} for different q_e and q_{lac} to maximize osmotic comfort with lens wear without compromising hypoxic safety (Kim et al., 2020) and lens adhesion (Cerretani et al., 2012).

Although the best available data were used to determine osmolarity of the various tear compartments, more information on tear-evaporation flux during lens wear for normal and dry eyes and a better understanding of the evaporation-flux difference between PrLTF and PrCjTF is needed. As discussed in Section 2.5, tear-evaporation rates depend strongly on the environmental humidity, airflow velocity, and temperature. Therefore, future measurements should be made with flow evaporimeters [e.g. Peng et al. (2014b)] rather than with closed-chamber evaporimeters widely used in the past.

We determined that the upper- and lower-meniscus osmolarities exhibit negligible salinity differences for complete blinks. Gad et al. (2019) found no difference in upper and lower meniscus osmolarities for normal-eye lens wear but, however, found a significant difference between the upper and lower menisci osmolarities in symptomatic lens-wearing group during lens wear. It is difficult to justify this latter result. Measurement difficulties arise in the detection of upper meniscus osmolarities and/or in the known low sensitivity of the TearLab (TearLab Corp., San Diego, CA, USA) instrument (Szalai et al., 2012). Another possibility is that symptomatic contact-lens wearers experience more frequent incomplete blinks leading to imperfect mixing of the tear. In such a case, the majority of the hyperosmotic tear film mixes with the upper meniscus resulting in higher osmolarity than that of the lower meniscus. Further investigation on upper and lower menisci osmolarity is warranted.

Similar to tear-evaporation rates, the effect of SCL wear on tear-production and tear-drainage rates also requires further research. For instance, cold receptors are thought to influence basal tear production (Belmonte and Gallar, 2011). SCLs can potentially act as a thermal insulator to the ocular surface thereby affecting basal tear production. The recently devised modified-Schirmer tear test (Kim et al., 2019; Li et al., 2018; Telles et al., 2017) allows direct measurement of tear-production rates for the first time. Further clinical studies are necessary to understand the difference in tear-production rates between normal and dry eyes and between no lens and lens wear. To date, tear-drainage rate has only been determined with physical models (Zhu and Chauhan, 2005) or calculated from clinically measured tear-turnover rates (Tomlinson and Khanal, 2005). However, tear-drainage rates calculated from tear-turnover rates assume that the volume of PrCTF remains constant and does not influence the fluorescein-dye concentration. With accurate tear-production and tear-evaporation rates in hand, tear-drainage rates can theoretically be determined without measuring the tear-turnover rate. Additional research is needed to establish whether tear-production and tear-drainage rates are altered by SCL wear. With more information on tear dynamics for normal and dry eyes including as well as no-lens and lens wear, precise calculation of tear-compartment osmolarities is possible.

Spatially localized variance in salt osmolarity (e.g., due to random local lipid-layer breakup on the PrLTF) within each tear-film compartment is not included in the current tear-dynamics model. With no-lens wear, mathematical studies showed that local PrCTF osmolarity can reach 600–900 mOsM in areas with lipid-layer breakup during a 10-s interblink period (Braun et al., 2015; Peng et al., 2014a). The effect of

localized PrLTF osmolarity spikes on the PoLTF and the importance of localized spikes on ocular-surface discomfort remains unknown.

Our tear-dynamics model analysis of tear-compartment osmolarities reveals the major differences in osmolarities of the tear compartments during SCL wear. These differences potentially explain why no correlation has been found between clinically measured meniscus osmolarity and SCL wear discomfort (Chen et al., 2013; Golebiowski et al., 2017; İskeleli et al., 2002; Sarac et al., 2012; Stahl et al., 2009). Here, we demonstrate that careful design of SCLs, specifically lowering lens-salt diffusivity, can lower PoLTF osmolarity and can protect the cornea from hyperosmotic stress.

Author statement

Young Hyun Kim: Methodology, Software, Validation, Formal analysis, Investigation, Writing – original draft, Writing - review & editing, Visualization. Thien Nguyen: Software, Investigation, Data curation, Visualization. Meng C. Lin: Formal analysis, Writing – original draft, Writing - review & editing. Cheng-Chun Peng: Methodology, Software, Formal analysis, Writing – original draft, Writing - review & editing. Clayton J. Radke: Conceptualization, Methodology, Formal analysis, Resources, Writing – original draft, Writing - review & editing, Supervision, Project administration, Funding acquisition.

Declarations of interest

Coopervision, Inc. (CJR, C-CP, MCL)

Acknowledgements

This work was supported by CooperVision Inc. (No Commercial Interest). Dr. Colin Cerretani kindly provided a preliminary code (Cerretani and Radke, 2014).

Appendices.

Appendix A. Determination of the exposed surface-area fraction (α) of bulbar conjunctiva

To determine α, the surface-area fraction of bulbar conjunctiva not covered by the contact lens or the eyelids, we used a SCL radius of 7.0 mm as our lens geometry (Chauhan and Radke, 2001). Using Comsol Multiphysics 5.5 platform (Comsol Inc, Burlington, MA, USA), a 2-dimensional computer-aided design of the ocular surface and lids was performed based on the measurements of Malbouisson et al. (2000). Geometries of the cornea and eyelids were modified to ensure that the area of bulbar conjunctiva exposed to the environment (A_{cj}) and cornea (A_{cn}) matched those of Cerretani and Radke (2014). Then, in the design, the contact lens was placed on top of the ocular surface to determine the area of the exposed bulbar conjunctiva that was underneath the lens. The area of bulbar conjunctiva covered by the contact lens and not by the eyelid ($A_{cj,lens}$) was 24.1 mm^2. Meanwhile, the total bulbar conjunctiva that was uncovered by the eyelid was 105.1 mm^2. Since α is the surface-area fraction of bulbar conjunctiva exposed to air, (1- α) represents for the fraction of bulbar conjunctiva that is underneath the contact lens and not covered by the eyelid. This gives the following expression

$$\alpha = 1 - \frac{A_{cj,lens}}{A_{cj}} \tag{A1}$$

Evaluation of Equation (A1) gives $\alpha = 0.77$.

Appendix B. Lens water flux

We assume that salt diffusion through the lens does not materially influence opposing osmotic-driven water hydrodynamic flow. Water flux is governed by a modified Darcy law (Brenner and Edwards, 1993)

$$J_{w,lens} = \widetilde{J}_{w,lens} c_{w,lens} = -\frac{K}{\mu_w} \frac{(\Delta P - \Delta \Pi)}{h_{lens}} c_{w,lens} \tag{B1}$$

where, $J_{w,lens}$ is the molar flux of water through the lens, $\widetilde{J}_{w,lens}$ is the volumetric water flux (or the superficial velocity), $c_{w,lens}$ is the water concentration per unit lens volume, K is the Darcy hydraulic permeability of the lens, μ_w is tear viscosity, P is applied pressure, $\Pi = 2RTc$ is the osmotic pressure, R is the gas constant, c is the aqueous salt concentration, and h_{lens} is the lens thickness. Here, $c_{w,lens} = \phi_w 55.85M$ is the water concentration within the lens, and ϕ_w is the water volume fraction of the lens (Dursch et al., 2014). We used a ϕ_w of 0.38 based on the works of Hoch et al. (2003) and Guan et al. (2011). Since water flow within the lens is osmotic driven and not due to an applied pressure difference and because we assume constant water concentration within the lens, Equation (B1) reduces to

$$J_{w,lens} = \frac{2KRT}{\mu_w} \frac{(c_{PrL} - c_{PoL})}{h_{lens}} c_{w,lens} \tag{B2}$$

where, c_{PrL} and c_{PoL} are tear salt concentrations at the PrLTF and PoLTF interfaces, respectively. The factor of two is required because water flux depends on the salt osmotic concentration and not molar salt concentration. Division of Equation (B2) by $c_{w,lens}$ gives the volumetric water flux as

$$\widetilde{J}_{w,lens} = v_w = \frac{2KRT}{\mu_w} \frac{(c_{PrL} - c_{PoL})}{h_{lens}} \tag{B3}$$

where v_w is the superficial velocity. Determined $\widetilde{J}_{w,lens}$ values for the three chosen lens-salt diffusivities are provided in Table B1 for normal (Fig. 10) and dry-eye (Fig. 11) analyses.

Appendix C. Lens-molar salt flux

The counter flux of water in Equation (B3) induces a convective term in addition to diffusion for the salt flux across a lens. Transient salt mass conservation demands the following expression, where the lens-salt flux, $J_{s,lens}$, is given in Equation (11) of the main text,

$$\frac{\partial c_{lens}}{\partial t} + \nabla \cdot J_{s,lens} = 0 \tag{C1}$$

where ∇ is the divergence operator. Therefore, Equation (C1) reads

$$\frac{\partial c_{lens}}{\partial t} + \widetilde{J}_{w,lens}\frac{\partial c_{lens}}{\partial z} = D_s\frac{\partial^2 c_{lens}}{\partial z^2} \tag{C2}$$

where c_{lens} is the local salt concentration per unit lens volume within the lens, z is the spatial location within the lens directed from the posterior to anterior surface, $\widetilde{J}_{w,lens}$ is the superficial water velocity defined in Equation (B3), D_s is the lens-salt diffusivity, and t is time. Equation (C2) is given in the main text as Equation (10).

To assess whether the salt flux due to $\widetilde{J}_{w,lens}$ is important compared to that of salt diffusion, we determined the Péclet number (*Pe*) for the three salt diffusivities used for both normal (Fig. 10) and dry-eye (Fig. 11) conditions. The Péclet number is a dimensionless ratio of convective transport and diffusive transport rates and is expressed by the following definition

$$Pe \equiv \frac{\widetilde{J}_{w,lens}h_{lens}}{D_s} \tag{C3}$$

where h_{lens} is the lens thickness. Averaged $\widetilde{J}_{w,lens}$ for the periodic steady state from Appendix B is used to calculate the Péclet number as enumerated in Table C1. Following Figs. 10 and 11, h_{lens} for the Péclet number is set as 60 μm. Since the Péclet number is very small for all relevant conditions, salt transport across the lens due to counter-water transport $\widetilde{J}_{w,lens}$ is negligible. Thus, Equation (C2) simplifies to Fick's second law

$$\frac{\partial c_{lens}}{\partial t} = D_s\frac{\partial^2 c_{lens}}{\partial z^2} \tag{C4}$$

Likewise, $\widetilde{J}_{w,lens}$ in Equation (11) is negligible for assessing the lens salt flux at the anterior and posterior surfaces of the lens.

Appendix D. Tear supply from the lacrimal gland during the blink phase

The blink phase includes both deposition and eyelid-closure phases. The elapsed time for this process is ~0.2 s (Cerretani and Radke, 2014). We lump the lacrimal-production rate during the blink phase as

$$V_{blink} = 0.2q_{lac} \tag{D1}$$

where q_{lac} varies and can be found in Table 2.

Appendix E. Salt diffusion from non-perched PrLTF to menisci and PrCjTF

Although formation of tear-menisci black lines upon lid opening perches or isolates the PrLTF and PrCjTFs, lack of visualization of black lines in some subjects makes a non-isolated tear possible. Therefore, salt flux from the tear film to the adjacent tear menisci during the interblink period was investigated. We picture a thin but non-perched tear film directly connected to a meniscus. Salt diffusion from the PrLTF to a meniscus follows Fick's second law or

$$\frac{\partial c}{\partial t} = D_\infty\frac{\partial^2 c}{\partial x^2} \tag{E1}$$

where c is aqueous salt concentration, D_∞ is the bulk diffusion constant of salt in water, and x is the spatial coordinate to the center of the PrLTF directed from the menisci. Thus, $x = 0$ is the interface between PrLTF and the meniscus while $x = \lambda$ is located at the center of the PrLTF. The requisite boundary conditions are

$$c(0, x) = c_{im} \tag{E2}$$

$$c(t, 0) = c_{im} \tag{E3}$$

$$c(t, \lambda) = c_{PrL} \tag{E4}$$

Equations (E1) – (E4) are nondimensionalized as $\theta = (c - c_{im})/(c_{PrL} - c_{im})$, $\mathrm{X} = x/\lambda$, and $\tau = D_\infty t/\lambda^2$. The nondimensionalized partial differential equation is solved using Laplace transformations to obtain

$$\overline{\theta}(s, \mathrm{X}) = \frac{1}{s}\frac{\sinh(\sqrt{s}\,\mathrm{X})}{\sinh(\sqrt{s})} \tag{E5}$$

where $\overline{\theta}$ is the Laplace dimensionless concentration and s is the Laplace variable. At early time, Equation (E5) inverts to

$$\theta(\tau, \mathrm{X}) = erfc\left[\frac{(1-\mathrm{X})}{2\sqrt{\tau}}\right] \tag{E6}$$

Since salt flux, $J_{s,Bl} = -D_{\infty}\frac{\partial c}{\partial x} = -\left[\frac{D_{\infty}}{\lambda}(c_{PrL} - c_{im})\right]\frac{\partial \theta}{\partial X}$, the flux at X = 0 can be solved to yield the magnitude of salt flux from the tear film to the meniscus as

$$J_{s,Bl} = \frac{D_{\infty}}{\sqrt{\pi\tau}\lambda}[c_{PrL} - c_{im}]e^{-1/(4\tau)} \tag{E7}$$

Since upper and lower menisci have approximately the same concentration, c_{im} is the concentration of either meniscus. To assess the influence of a non-perched tear film, $J_{s,Bl}h_{um}L_{um,PrL} + J_{s,Bl}h_{lm}L_{lm,PrL}$ is subtracted from the right side of Equation (8), $J_{s,Bl}h_{um}L_{um,PrCj} + J_{s,Bl}h_{lm}L_{lm,PrCj}$ is subtracted from the right side of Equation (6), and the subtracted upper and lower meniscus terms are added to Equation (4) for upper and lower meniscus balances, respectively. h_{um} and h_{im} are upper and lower meniscus heights, respectively, $L_{um,PrL}$ and $L_{lm,PrL}$ are arc lengths of upper and lower eyelids at the PrLTF region, respectively, and $L_{um,PrCj}$ and $L_{lm,PrCj}$ are arc lengths of upper and lower eyelids at the PrCjTF region, respectively. Arc lengths and meniscus heights are determined from Appendix A of Cerretani and Radke (2014). We find that lack of a perched tear film results in a negligible difference in our tear-compartment osmolarities. Since the tear-compartment osmolarities do not change due to diffusion from PrLTF to tear menisci during the interblink, diffusion from the PrLTF to the PrCjTF is also neglected.

Table B1
Averaged volumetric water flux for various salt-diffusivity contact lenses

NORMAL/DRY EYE	SALT DIFFUSIVITY D_s (cm^2/s)	Volumetric Water Flux $\bar{J}_{w,lens}$ (m/s)
Normal	2.8×10^{-8}	2.9×10^{-9}
Normal	1.1×10^{-6}	4.4×10^{-10}
Normal	6.0×10^{-6}	9.2×10^{-11}
Dry	2.8×10^{-8}	8.2×10^{-9}
Dry	1.1×10^{-6}	1.3×10^{-9}
Dry	6.0×10^{-6}	2.6×10^{-10}

Table C1
Péclet number for various salt-diffusivity contact lenses

NORMAL/DRY EYE	SALT DIFFUSIVITY (cm^2/s)	PÉCLET NUMBER
Normal	2.8×10^{-8}	6.6×10^{-2}
Normal	1.1×10^{-6}	2.6×10^{-4}
Normal	6.0×10^{-6}	9.6×10^{-6}
Dry	2.8×10^{-8}	1.8×10^{-1}
Dry	1.1×10^{-6}	7.2×10^{-4}
Dry	6.0×10^{-6}	2.7×10^{-5}

References

Alghamdi, W.M., Markoulli, M., Holden, B.A., Papas, E.B., 2016. Impact of duration of contact lens wear on the structure and function of the meibomian glands. Ophthalmic Physiol. Opt. 36, 120–131.

Amparo, F., Jin, Y., Hamrah, P., Schaumberg, D.A., Dana, R., 2014. What is the value of incorporating tear osmolarity measurement in assessing patient response to therapy in dry eye disease? Am. J. Ophthalmol. 157, 69–77 e2.

Amsden, B., 1998. Solute diffusion within hydrogels. Mechanisms and models. Macromolecules 31, 8382–8395.

Arita, R., Itoh, K., Inoue, K., Kuchiba, A., Yamaguchi, T., Amano, S., 2009. Contact lens wear is associated with decrease of meibomian glands. Ophthalmology 116, 379–384.

Badugu, R., Jeng, B.H., Reece, E.A., Lakowicz, J.R., 2018. Contact lens to measure individual ion concentrations in tears and applications to dry eye disease. Anal. Biochem. 542, 84–94.

Baudouin, C., Aragona, P., Messmer, E.M., Tomlinson, A., Calonge, M., Boboridis, K.G., Akova, Y.A., Geerling, G., Labetoulle, M., Rolando, M., 2013. Role of hyperosmolarity in the pathogenesis and management of dry eye disease: Proceedings of the OCEAN group meeting. Clin Sci 11, 246–258.

Belmonte, C., Gallar, J., 2011. Cold thermoreceptors, unexpected players in tear production and ocular dryness sensations. Invest. Ophthalmol. Vis. Sci. 52, 3888–3892.

Berg, J.C., 2009. An Introduction to Interfaces and Colloids: The Bridge to Nanoscience. World Scientific Publishing Co. Pte. Ltd., Singapore. Chapter II.

Boushehri, A., Tang, D., Shieh, K.J., Prausnitz, J.M., Radke, C.J., 2010. Water transport through soft contact lenses determined in a fan-evaporation cell. J. Membr. Sci. 362, 529–534.

Brady, J., 1994. Hindered diffusion. In: AIChE Annual Meeting. San Francisco, CA, p. 320.

Braun, R.J., King-Smith, P.E., Begley, C.G., Li, L., Gewecke, N.R., 2015. Dynamics and function of the tear film in relation to the blink cycle. Prog. Retin. Eye Res. 45, 132–164.

Brenner, H., Edwards, D.A., 1993. Macrotransport Processes. Butterworth-Heinemann, Boston.

Bretherton, F.P., 1961. The motion of long bubbles in tubes. J. Fluid Mech. 10, 166–168.

Bron, A.J., Tiffany, J.M., Yokoi, N., Gouveia, S.M., 2002. Using osmolarity to diagnose dry eye: A compartmental hypothesis and review of our assumptions. Adv. Exp. Med. Biol. 506, 1087–1095.

Cedarstaff, T.H., Tomlinson, A., 1983. A comparative study of tear evaporation rates and water content of soft contact lenses. Am. J. Optom. Physiol. Opt 60, 167–174.

Cerretani, C.F., Radke, C.J., 2014. Tear dynamics in healthy and dry eyes. Curr. Eye Res. 39, 580–595.

Cerretani, C., Peng, C.C., Chauhan, A., Radke, C.J., 2012. Aqueous salt transport through soft contact lenses: An osmotic-withdrawal mechanism for prevention of adherence. Contact Lens Anterior Eye 35, 260–265.

Chauhan, A., Radke, C.J., 2001. Modeling the vertical motion of a soft contact lens. Curr. Eye Res. 22, 102–108.

Chen, Q., Wang, J., Shen, M., Cui, L., Cai, C., Li, M., Li, K., Lu, F., 2011. Tear menisci and ocular discomfort during daily contact lens wear in symptomatic wearers. Invest. Ophthalmol. Vis. Sci. 52, 2175–2180. https://doi.org/10.1167/iovs.10-5780.

Chen, S.P., Massaro-Giordano, G., Pistilli, M., Schreiber, C.A., Bunya, V.Y., 2013. Tear osmolarity and dry eye symptoms in women using oral contraception and contact lenses. Cornea 32, 423–428.
Chiou, J.C., 2019. The development of smart contact lens system: Taking dry eye syndrome diagnosis as an example, in: Future Tech Expo.
Craig, J.P., Tomlinson, A., 1997. Importance of the lipid layer in human tear film stability and evaporation. Optom. Vis. Sci. 74, 8–13.
Craig, J.P., Willcox, M.D.P., Argüeso, P., Maissa, C., Stahl, U., Tomlinson, A., Wang, J., Yokoi, N., Stapleton, F., 2013. The TFOS international workshop on contact lens discomfort: Report of the contact lens interactions with the tear film subcommittee. Invest. Ophthalmol. Vis. Sci. 54, TFOS123–TFOS156. https://doi.org/10.1167/iovs.13-13235.
Creech, J.L., Chauhan, A., Radke, C.J., 2001. Dispersive mixing in the posterior tear film under a soft contact lens. Ind. Eng. Chem. Res. 40, 3015–3026.
Dartt, D.A., 2002. Regulation of mucin and fluid secretion by conjunctival epithelial cells. Prog. Retin. Eye Res. 21, 555–576.
Dartt, D.A., Willcox, M.D.P., 2013. Complexity of the tear film: Importance in homeostasis and dysfunction during disease. Exp. Eye Res. 117, 1–3. https://doi.org/10.1016/j.exer.2013.10.008.
del Águila-Carrasco, A.J., Ferrer-Blasco, T., García-Lázaro, S., Esteve-Taboada, J.J., Montés-Micó, R., 2015. Assessment of corneal thickness and tear meniscus during contact-lens wear. Contact Lens Anterior Eye 38, 185–193. https://doi.org/10.1016/j.clae.2015.01.010.
Doane, M.G., 1981. Blinking and the mechanics of the lacrimal drainage system. Ophthalmology 88, 844–851.
Dursch, T.J., Taylor, N.O., Liu, D.E., Wu, R.Y., Prausnitz, J.M., Radke, C.J., 2014. Water-soluble drug partitioning and adsorption in HEMA/MAA Hydrogels. Biomaterials 35, 620–629.
Ehlers, N., 1965. The precorneal film. Biomicroscopical, histological and chemical investigations. Acta Ophthalmol. 1–134.
Farris, R.L., 1986. Tear osmolarity variation in the dry eye. Trans. Am. Ophthalmol. Soc. 84, 250–268.
Farris, R.L., Stuchell, R.N., Mandell, D., 1981. Basal and reflex human tear analysis: I. Physical measurements: osmolarity, basal volumes and reflex flow rate. Ophthalmology 88, 852–857.
Farris, R.L., Gilbard, J.P., Stuchell, R.N., Mandel, I.D., 1983. Diagnostic tests in keratoconjunctivitis sicca. CLAO J. 9, 23–28.
Fatt, I., 1991. Observations of tear film break up on model eyes. CLAO J. 17, 267–281.
Fatt, I., Weissman, B.A., 1992. Physiology of the Eye. An Introduction to the Vegetative Functions, second ed. Butterworth-Heinemann, Boston. Chapter 10.
Finnemore, V.M., Korb, D.R., Greiner, J.V., Glonek, T., Herman, J.P., 1998. Fluorescein dye concentration as a factor in tear film fluorescence. In: Sullivan, D.A., Dartt, D.A., Meneray, M.A. (Eds.), Lacrimal Gland, Tear Film, and Dry Eye Syndromes 2. Springer, Boston, MA, pp. 875–878. https://doi.org/10.1007/978-1-4615-5359-5_123.
Fraunfelder, F.T., 1976. Extraocular fluid dynamics: How best to apply topical ocular medication. Trans. Am. Ophthalmol. Soc. 74, 457–487.
Gad, A., Vingrys, A.J., Wong, C.Y., Jackson, D.C., Downie, L.E., 2019. Tear film inflammatory cytokine upregulation in contact lens discomfort. Ocul. Surf. 17, 89–97. https://doi.org/10.1016/j.jtos.2018.10.004.
Gaffney, E.A., Tiffany, J.M., Yokoi, N., Bron, A.J., 2010. A mass and solute balance model for tear volume and osmolarity in the normal and the dry eye. Prog. Retin. Eye Res. 29, 59–78.
Gilbard, J.P., 1985. Tear film osmolarity and keratoconjunctivitis sicca. CLAO J. 11, 243–250.
Gilbard, J.P., 1994. Human tear film electrolyte concentrations in health and dry eye disease. Int. Ophthalmol. Clin. 34, 27–36.
Gilbard, J.P., Farris, R.L., Santamaria II., J., 1978. Osmolarity of tear micro volumes in keratoconjunctivitis sicca. Arch. Ophthalmol. 96, 677–681.
Gilbard, J.P., Carter, J.B., Sang, D.N., Refojo, M.F., Hanninen, L.A., Kenyon, K.R., 1984. Morphologic effect of hyperosmolarity on rabbit corneal epithelium. Ophthalmology 91, 1205–1212.
Gilbard, J.P., Rossi, S.R., Gray, K.L., Hanninen, L.A., Kenyon, K.R., 1988. Tear film osmolarity and ocular surface disease in two rabbit models for keratoconjunctivitis sicca. Invest. Ophthalmol. Vis. Sci. 29, 374–378.
Glasson, M.J., Stapleton, F., Keay, L., Willcox, M.D.P., 2006. The effect of short term contact lens wear on the tear film and ocular surface characteristics of tolerant and intolerant wearers. Contact Lens Anterior Eye 29, 41–47.
Golebiowski, B., Chao, C., Stapleton, F., Isabelle, J., 2017. Corneal nerve morphology, sensitivity, and tear neuropeptides in contact lens wear. Optom. Vis. Sci. 94, 534–542.
Guan, L., González Jiménez, M.E., Walowski, C., Boushehri, A., Prausnitz, J.M., Radke, C. J., 2011. Permeability and partition coefficient of aqueous sodium chloride in soft contact lenses. J. Appl. Polym. Sci. 122, 1457–1471.
Guillon, M., Maissa, C., 2008. Contact lens wear affects tear film evaporation. Eye Contact Lens 34, 326–330.
Guzmán, M., Miglio, M., Keitelman, I., Shiromizu, C.M., Sabbione, F., Fuentes, F., Trevani, A.S., Giordano, M.N., Galletti, J.G., 2020. Transient tear hyperosmolarity disrupts the neuroimmune homeostasis of the ocular surface and facilitates dry eye onset. Immunology 161, 148–161. https://doi.org/10.1111/imm.13243.
Hamano, H., Hori, M., Mitsunaga, S., 1981. Measurement of evaporation rate of water from the precorneal tear film and contact lenses. Contact 25, 8–14.
Hirata, H., Rosenblatt, M.I., 2014. Hyperosmolar tears enhance cooling sensitivity of the corneal nerves in rats: Possible neural basis for cold-induced dry eye pain. Invest. Ophthalmol. Vis. Sci. 55, 5821–5833.
Hirata, H., Oshinsky, M., Fried, N., 2013. Short exposure to intense tear hyperosmolarity leads to functional alterations of the corneal nerves involved in tearing and/or ocular pain: Implications for dry eye disease. Invest. Ophthalmol. Vis. Sci. 54, 2193.
Hirata, H., Mizerska, K., Marfurt, C.F., Rosenblatt, M.I., 2015. Hyperosmolar tears induce functional and structural alterations of corneal nerves: Electrophysiological and anatomical evidence toward neurotoxicity. Invest. Ophthalmol. Vis. Sci. 56, 8125–8140.
Hoch, G., Chauhan, A., Radke, C.J., 2003. Permeability and diffusivity for water transport through hydrogel membranes. J. Membr. Sci. 214, 199–209. https://doi.org/10.1016/S0376-7388(02)00546-X.
İskeleli, G., Karakoç, Y., Aydn, O., Yetik, H., Uslu, H., Kzlkaya, M., 2002. Comparison of tear-film osmolarity in different types of contact lenses. CLAO J. 28, 174–176.
Jones, L., Hui, A., Phan, C.-M., Read, M.L., Azar, D., Buch, J., Ciolino, J.B., Naroo, S.A., Pall, B., Romond, K., Sankaridurg, P., Schnider, C.M., Terry, L., Willcox, M., 2021. CLEAR - Contact lens technologies of the future. Contact Lens Anterior Eye 44, 398–430.
Kedem, O., Katchalsky, A., 1958. Thermodynamic analysis of the permeability of biological membranes to non-electrolytes. Biochim. Biophys. Acta 27, 229–246. https://doi.org/10.1016/0006-3002(58)90330-5.
Khanal, S., Tomlinson, A., McFadyen, A., Diaper, C., Ramaesh, K., 2008. Dry eye diagnosis. Invest. Ophthalmol. Vis. Sci. 49, 1407–1414.
Khanal, S., Tomlinson, A., Diaper, C.J.M., 2009. Tear physiology of aqueous deficiency and evaporative dry eye. Optom. Vis. Sci. 86, 1235–1240.
Kim, J., Kim, M., Lee, M.-S., Kim, K., Ji, S., Kim, Y.-T., Park, J., Na, K., Bae, K.-H., Kyun Kim, H., Bien, F., Young Lee, C., Park, J.-U., 2017. Wearable smart sensor systems integrated on soft contact lenses for wireless ocular diagnostics. Nat. Commun. 8, 14997.
Kim, Y.H., Graham, A.D., Li, W., Radke, C.J., Lin, M.C., 2019. Human lacrimal production rate and wetted length of modified Schirmer's tear test strips. Transl Vis Sci Technol 8, 40. https://doi.org/10.1167/tvst.8.3.40.
Kim, Y.H., Lin, M.C., Radke, C.J., 2020. Limbal metabolic support reduces peripheral corneal edema with contact-lens wear. Transl Vis Sci Technol 9, 44. https://doi.org/10.1167/tvst.9.7.44.
Kimball, S.K., King-Smith, P.E., Nichols, J.J., 2010. Evidence for the major contribution of evaporation to tear film thinning between blinks. Invest. Ophthalmol. Vis. Sci. 51, 6294–6297.
King-Smith, P.E., Fink, B.A., Fogt, N., Nichols, K.K., Hill, R.M., Wilson, G.S., 2000. The thickness of the human precorneal tear film: Evidence from reflection spectra. Invest. Ophthalmol. Vis. Sci. 41, 3348–3359.
King-Smith, P.E., Hinel, E.A., Nichols, J.J., 2010. Application of a novel interferometric method to investigate the relation between lipid layer thickness and tear film thinning. Invest. Ophthalmol. Vis. Sci. 51, 2418–2423.
Kojima, T., Matsumoto, Y., Ibrahim, O.M.A., Wakamatsu, T.H., Uchino, M., Fukagawa, K., Ogawa, J., Dogru, M., Negishi, K., Tsubota, K., 2011. Effect of controlled adverse chamber environment exposure on tear functions in silicon hydrogel and hydrogel soft contact lens wearers. Invest. Ophthalmol. Vis. Sci. 52, 8811–8817.
Kok, J.H.C., Boets, E.P.M., van Best, J.A., Kijlstra, A., 1992. Fluorophotometric assessment of tear turnover under rigid contact lenses. Cornea 11, 515–517.
Korb, D.R., Greiner, J.V., Glonek, T., Whalen, A., Hearn, S.L., Esway, J.E., Leahy, C.D., 1998. Human and rabbit lipid layer and interference pattern observations. In: Sullivan, D.A., Dartt, D.A., Meneray, M.A. (Eds.), Lacrimal Gland, Tear Film, and Dry Eye Syndromes 2. Springer, Boston, MA, pp. 305–308.
Lemp, M.A., Bron, A.J., Baudouin, C., Benítez del Castillo, J.M., Geffen, D., Tauber, J., Foulks, G.N., Pepose, J.S., Sullivan, B.D., 2011. Tear osmolarity in the diagnosis and management of dry eye disease. Am. J. Ophthalmol. 151, 792-798.E1. https://doi.org/10.1016/j.ajo.2010.10.032.
Leung, B.K., Bonanno, J.A., Radke, C.J., 2011. Oxygen-deficient metabolism and corneal edema. Prog. Retin. Eye Res. 30, 471–492.
Li, D.-Q., Luo, L., Chen, Z., Kim, H.-S., Song, X.J., Pflugfelder, S.C., 2006. JNK and ERK MAP kinases mediate induction of IL-1β, TNF-α and IL-8 following hyperosmolar stress in human limbal epithelial cells. Exp. Eye Res. 82, 588–596.
Li, S., Kim, Y.H., Li, W., Lin, M.C., Radke, C.J., 2018. Human lacrimal production rates from modified Schirmer-tear test. Optom. Vis. Sci. 95, 343–348.
Lin, M.C., Soliman, G.N., Song, M.J., Smith, J.P., Lin, C.T., Chen, Y.Q., Polse, K.A., 2003. Soft contact lens extended wear affects corneal epithelial permeability: Hypoxic or mechanical etiology? Contact Lens Anterior Eye 26, 11–16. https://doi.org/10.1016/S1367-0484(02)00088-7.
Lin, M.C., Soliman, G.N., Lim, V.A., Giese, M.L., Wofford, L.E., Marmo, C., Radke, C.J., Polse, K.A., 2006. Scalloped channels enhance tear mixing under hydrogel contact lenses. Optom. Vis. Sci. 83, 874–878.
Liu, H., Begley, C., Chen, M., Bradley, A., Bonanno, J., McNamara, N.A., Nelson, J.D., Simpson, T., 2009. A link between tear instability and hyperosmolarity in dry eye. Invest. Ophthalmol. Vis. Sci. 50, 3671–3679.
Liu, D.E., Kotsmar, C., Nguyen, F., Sells, T., Taylor, N.O., Prausnitz, J.M., Radke, C.J., 2013. Macromolecule sorption and diffusion in HEMA/MAA hydrogels. Ind. Eng. Chem. Res. 52, 18109–18129.
Luo, L., Li, D.-Q., Corrales, R.M., Pflugfelder, S.C., 2005. Hyperosmolar saline is a proinflammatory stress on the mouse ocular surface. Eye Contact Lens 31, 186–193.
Machalińska, A., Zakrzewska, A., Adamek, B., Safranow, K., Wiszniewska, B., Parafiniuk, M., Machaliński, B., 2015. Comparison of morphological and functional meibomian gland characteristics between daily contact lens wearers and nonwearers. Cornea 34, 1098–1104.
Maki, K.L., Braun, R.J., Ucciferro, P., Henshaw, W.D., King-Smith, P.E., 2010. Tear film dynamics on an eye-shaped domain. Part 2. Flux boundary conditions. J. Fluid Mech. 647, 361–390.

Malbouisson, J.M., Baccega, A., Cruz, A., 2000. The geometrical basis of the eyelid contour. Ophthalmic Plast Recons 16, 427–431.
Mann, A., Sáez-Martinez, V., Lydon, F., Tighe, B., 2019. Investigating the permeation properties of contact lenses and its influence on tear electrolyte composition. J. Biomed. Mater. Res. B 107, 1997–2005. https://doi.org/10.1002/jbm.b.34291.
Martin, D.K., 1987. Osmolality of the tear fluid in the contralateral eye during monocular contact lens wear. Acta Ophthalmol. 65, 551–555.
Mathers, W.D., Lane, J.A., Sutphin, J.E., Zimmerman, M.B., 1996. Model for ocular tear film function. Cornea 15, 110–119.
McCulley, J.P., Shine, W., 1997. A compositional based model for the tear film lipid layer. Trans. Am. Ophthalmol. Soc. 95, 79–93.
McDonald, J.E., Brubaker, S., 1971. Meniscus-induced thinning of tear films. Am. J. Ophthalmol. 72, 139–146.
McMonnies, C.W., 2020. Aqueous deficiency is a contributor to evaporation-related dry eye disease. Eye Vis 7, 6.
McNamara, N.A., Polse, K.A., Brand, R.J., Graham, A.D., Chan, J.S., McKenney, C.D., 1999. Tear mixing under a soft contact lens: Effects of lens diameter. Am. J. Ophthalmol. 127, 659–665.
Miller, K.L., Polse, K.A., Radke, C.J., 2002. Black-line formation and the "perched" human tear film. Curr. Eye Res. 25, 155–162. https://doi.org/10.1076/ceyr.25.3.155.13478.
Mishima, S., Gasset, A., Klyce, S.D., Baum, J.L., 1966. Determination of tear volume and tear flow. Invest. Ophthalmol. Vis. Sci. 5, 264–276.
Mishima, S., Kubota, Z., Farris, R.L., 1971. The tear flow dynamics in normal and in keratoconjunctivitis sicca cases. Excepta Med 1801–1805.
Monticelli, M.V., Chauhan, A., Radke, C.J., 2005. The Effect of water hydraulic permeability on the settling of a soft contact lens on the eye. Curr. Eye Res. 30, 329–336. https://doi.org/10.1080/02713680590934085.
Nagyová, B., Tiffany, J.M., 1999. Components responsible for the surface tensions of human tears. Curr. Eye Res. 19, 4–11.
Newman, J., Thomas-Alyea, K.E., 2004. Electrochemical Systems, 3rd ed. Wiley-Interscience, Hoboken. Appendix C.
Nichols, J.J., King-Smith, P.E., 2003. Thickness of the pre- and post-contact lens tear film measured in vivo by interferometry. Invest. Ophthalmol. Vis. Sci. 44, 68–77.
Nichols, J.J., Mitchell, G.L., King-Smith, P.E., 2005. Thinning rate of the precorneal and prelens tear films. Invest. Ophthalmol. Vis. Sci. 46, 2253–2361.
Nicolson, P., Baron, R., Charbrereck, P., Court, J., Domschkem, A., Griesser, H., Ho, A., Hopken, J., Laycock, B.G., Liu, Q., Lohmann, D., Meijs, G.F., Papaspiliotopoulos, E., Riffle, J.S., Schindhelm, K., Sweeney, D., Terry Jr., W.L., Vogt, J., Winterton, L.C., 1999. Extended wear ophthalmic lens. US Patent 5, 965,631.
Ogasawara, K., Tsuru, T., Mitsubayashi, K., Karube, I., 1996. Electrical conductivity of tear fluid in healthy persons and keratoconjunctivitis sicca patients measured by a flexible conductimetric sensor. Graefes Arch. Clin. Exp. Ophthalmol. 234, 542–546.
Ong, B.L., 1996. Relation between contact lens wear and meibomian gland dysfunction. Optom. Vis. Sci. 73, 208–210.
Peng, C.-C., Chauhan, A., 2012. Ion transport in silicone hydrogel contact lenses. J. Membr. Sci. 399–400, 95–105.
Peng, C.-C., Cerretani, C.F., Braun, R.J., Radke, C.J., 2014a. Evaporation-driven instability of the precorneal tear film. Adv Colloid Interfac 206, 250–264.
Peng, C.-C., Cerretani, C.F., Li, Y., Bowers, S., Shahsavarani, S., Lin, M.C., Radke, C.J., 2014b. Flow evaporimeter to assess evaporative resistance of human tear-film lipid layer. Ind. Eng. Chem. Res. 53, 18130–18139. https://doi.org/10.1021/ie5030497.
Pratt, K.C., Wakeham, W.A., 1977. Self-diffusion in water and monohydric alcohols. J. Chem. Soc. Faraday Trans. II 997–1002.
Quinn, T.M., Grodzinsky, A.J., 1993. Longitudinal modulus and hydraulic permeability of poly(methacrylic acid) gels: Effects of charge density and solvent content. Macromolecules 26, 4332–4338.
Refojo, M.F., 1965. Permeation of water through some hydrogels. J. Appl. Polym. Sci. 9, 3417–3426.
Refojo, M.F., Miller, D., Fiore, A., 1972. A new fluorescent stain for soft hydrophilic lens fitting. Arch. Ophthalmol. 82, 275–277.
Rolando, M., Refojo, M.F., 1983. Tear evaporimeter for measuring water evaporation rate from the tear film under controlled conditions in humans. Exp. Eye Res. 36, 25–33.
Rosenfeld, L., Cerretani, C.F., Leiske, D.L., Toney, M.F., Radke, C.J., Fuller, G.G., 2013. Structural and rheological properties of meibomian lipid. Invest. Ophthalmol. Vis. Sci. 54, 2720–2732.
Sarac, O., Gurdal, C., Bostanci-Ceran, B., Can, I., 2012. Comparison of tear osmolarity and ocular comfort between daily disposable contact lenses: Hilafilcon B hydrogel versus narafilcon A silicone hydrogel. Int. Ophthalmol. 32, 229–233.
Siddique, J.I., Braun, R.J., 2015. Tear film dynamics with evaporation, osmolarity and surfactant transport. Appl. Math. Model. 39, 255–269.
Stahl, U., Willcox, M.D.P., Naduvilath, T., Stapleton, F., 2009. Influence of tear film and contact lens osmolality on ocular comfort in contact lens wear. Optom. Vis. Sci. 86, 857–867.
Stapleton, F., Marfurt, C., Golebiowski, B., Rosenblatt, M., Bereiter, D., Begley, C., Dartt, D., Gallar, J., Belmonte, C., Hamrah, P., Willcox, M., 2013. The TFOS international workshop on contact lens discomfort: report of the subcommittee on neurobiology. Invest. Ophthalmol. Vis. Sci. 54. TFOS71–TFOS97.
Stern, M.E., Gao, J., Siemasko, K.F., Beuerman, R.W., Pflugfelder, S.C., 2004. The role of the lacrimal functional unit in the pathophysiology of dry eye. Exp. Eye Res. 78, 409–416. https://doi.org/10.1016/j.exer.2003.09.003.
Sullivan, D.A., 2004. Tearful relationships? Sex, hormones, the lacrimal gland, and aqueous-deficient dry eye. Ocul. Surf. 2, 92–123. https://doi.org/10.1016/S1542-0124(12)70147-7.
Svitova, T.F., Lin, M.C., 2010. Tear lipids interfacial rheology: Effect of lysozyme and lens care solutions. Optom. Vis. Sci. 87, 10–20.
Szalai, E., Berta, A., Szekanecz, Z., Szûcs, G., Módis, L., 2012. Evaluation of tear osmolarity in non-Sjögren and Sjögren syndrome dry eye patients with the TearLab system. Cornea 31, 867–871. https://doi.org/10.1097/ICO.0b013e3182532047.
Takatori, S.C., Radke, C.J., 2012. A quasi-2-dimensional model for respiration of the cornea with soft contact lens wear. Cornea 31, 405–417. https://doi.org/10.1097/ICO.0b013e31823f0930.
Tao, A., Cai, C., Shen, M., Wang, J., Chen, Z., Xu, S., Li, M., Lu, F., 2011. Tear menisci after overnight contact lens wear. Optom. Vis. Sci. 88, 1433–1438. https://doi.org/10.1097/OPX.0b013e3182303631.
Telles, R., Li, W., Dursch, T.J., Lin, M.C., Radke, C.J., 2017. Human tear-production rate from closed-eye Schirmer-strip capillary dynamics. Colloids Surf, A Physicochem Eng Asp 521, 61–68. https://doi.org/10.1016/j.colsurfa.2016.08.027.
Tiffany, J.M., 1991. The viscosity of human tears. Int. Ophthalmol. 15, 371–376.
Tiffany, J.M., Winter, N., Bliss, G., 1989. Tear film stability and tear surface tension. Curr. Eye Res. 8, 507–515.
Tomlinson, A., Khanal, S., 2005. Assessment of tear film dynamics: Quantification approach. Ocul. Surf. 3, 81–95.
Tomlinson, A., Khanal, S., Ramaesh, K., Diaper, C., McFadyen, A., 2006. Tear film osmolarity: Determination of a referent for dry eye diagnosis. Invest. Ophthalmol. Vis. Sci. 47, 4309–4315.
Tomlinson, A., Doane, M.G., McFadyen, A., 2009. Inputs and outputs of the lacrimal system: Review of production and evaporative loss. Ocul. Surf. 7, 186–198.
van Best, J.A., Benitez del Castillo, J.M., Coulangeon, L.-M., 1995. Measurement of basal tear turnover using a standardized protocol. Graefes Arch. Clin. Exp. Ophthalmol. 233, 1–7.
Wang, J., Fonn, D., Simpson, T.L., Jones, L., 2003. Precorneal and pre- and postlens tear film thickness measured indirectly with optical coherence tomography. Invest. Ophthalmol. Vis. Sci. 44, 2524–2528.
Wang, J., Jiao, S., Ruggeri, M., Shousha, M.A., Chen, Q., 2009. In situ visualization of tears on contact lens using ultra high resolution optical coherence tomography. Eye Contact Lens 35, 44–49. https://doi.org/10.1097/ICL.0b013e31819579f2.
Willcox, M.D.P., Argüeso, P., Georgiev, G.A., Holopainen, J.M., Laurie, G.W., Millar, T.J., Papas, E.B., Rolland, J.P., Schmidt, T.A., Stahl, U., Suarez, T., Subbaraman, L.N., Uçakhan, O.Ö., Jones, L., 2017. TFOS DEWS II tear film report. Ocul. Surf. 15, 366–403. https://doi.org/10.1016/j.jtos.2017.03.006.
Wong, H., Fatt, I., Radke, C.J., 1996. Deposition and thinning of the human tear film. J. Colloid Interface Sci. 184, 44–51.
Yasuda, H., Lamaze, C.E., Ikenberry, L.D., 1968. Permeability of solutes through hydrated polymer membranes. Part 1. Diffusion of sodium chloride. Makromol. Chem. 118, 19–35.
Yeh, T.N., Graham, A.D., Lin, M.C., 2015. Relationships among tear film stability, osmolarity, and dryness symptoms. Optom. Vis. Sci. 92, e264–e272.
Yetisen, A.K., Jiang, N., Castaneda Gonzalez, C.M., Erenoglu, Z.I., Deng, J., Dong, X., Stößer, S., Brischwein, M., Butt, H., Cordeiro, M.F., Jakobi, M., Hayden, O., Koch, A. W., 2020. Scleral lens sensor for ocular electrolyte analysis. Adv Mater 32, 1906762.
You, J., Willcox, M.D.P., Madigan, M.C., Wasinger, V., Schiller, B., Walsh, B.J., Graham, P.H., Kearsley, J.H., Li, Y., 2013. Tear fluid protein biomarkers. Adv. Clin. Chem. 62, 151–196.
Zhang, J., Begley, C.G., Situ, P., Simpson, T., Liu, H., 2017. A link between tear breakup and symptoms of ocular irritation. Ocul. Surf. 15, 696–703.
Zhu, H., Chauhan, A., 2005. A mathematical model for tear drainage through the canaliculi. Curr. Eye Res. 30, 621–630.

Glossary

a: Adjustable constant in lens salt diffusivity
a_f: Polymer strand characteristic radius (nm)
A_{cj}: Cross-sectional area of the bulbar conjunctiva that is not covered by the eyelids (cm^2)
$A_{cj.lens}$: Cross-sectional area of the bulbar conjunctiva covered by the contact lens and not by the eyelids (cm^2)
A_{cn}: Cross-sectional area of the cornea that is not covered by the eyelids (cm^2)
A_{eye}: Area of the eye that undergoes tear evaporation (cm^2)
A_{im}: Cross-sectional area of the meniscus. i = u and l indicate upper and lower menisci, respectively (cm^2)
A_{lens}: Cross-sectional area of the lens exposed to the environment (cm^2)
A_{skin}: Area of skin that is within the evaporimeter chamber (cm^2)
b: Adjustable constant in lens salt diffusivity
c: Salt concentration (mol/m^3)
c_{bulk}: Salt concentration of the tear film mixed during a blink phase (mol/m^3)
c_{blink}: Salt concentration of the tear produced by the lacrimal glands during the blink phase (mol/m^3)
c_{im}: Salt concentration of the meniscus. i = u and l indicate upper and lower menisci, respectively (mol/m^3)
c_{lens}: Salt concentration within the lens (mol/m^3)
c_{PoL}: Salt concentration in the post-lens tear film (mol/m^3)
c_{PrCj}: Salt concentration in the pre-conjunctival tear film (mol/m^3)
c_{PrL}: Salt concentration in the pre-lens tear film (mol/m^3)
c_{si}: Salt concentration of the conjunctival sac. i = u and l indicate upper and lower conjunctival sacs, respectively (mol/m^3)
$c_{w.lens}$: Water concentration within the lens (mol/m^3)
D_s: Diffusivity of salt in soft contact lens (cm^2/s)

D_∞: Diffusivity of salt in water (cm^2/s)
E_s: Salt enhancement factor
E_s^{el}: Enhancement factor for nonspecific electrostatic repulsion
E_s^{ex}: Enhancement factor for hard-sphere exclusion
E_s^{ad}: Enhancement factor for specific adsorption of salt to polymer chains
F: Gel hydrodynamic resistance factor
h_{im}: Meniscus height. i = u and l indicate upper and lower menisci, respectively (μm)
h_{lens}: Thickness of the soft contact lens (μm)
$h_{tf,j}$: Thickness of tear film. j = PrCj and j = PrL indicate PrCjTF and PrLTF, respectively (μm)
i: Subscript indicating upper (u) or lower (l)
j: Subscript indicating either pre-conjunctival tear film (PrCj) or pre-lens tear film (PrL)
$J_{s,Bl}$: Salt molar flux from tear film to menisci ($mol/(m^2 \times s)$)
$J_{s,lens}$: Salt molar flux across soft contact lens ($mol/(m^2 \times s)$)
$\widetilde{J}_{w,cj}$: Volumetric water flux from the bulbar conjunctiva (m/s)
$\widetilde{J}_{w,cn}$: Volumetric water flux from the cornea (m/s)
$\widetilde{J}_{w,e}$: Volumetric water evaporation flux (m/s)
$\widetilde{J}_{w,lens}$: Volumetric water flux across the soft contact lens (m/s)
$J_{w,lens}$: Molar water flux across the soft contact lens ($mol/(m^2 \times s)$)
k_s: Salt partition coefficient for soft contact lens
K: Darcy hydraulic permeability of water (m^2)
L: Membrane thickness (μm)
$L_{im,PrL}$: Arc length of eyelid at pre-lens tear-film region. i = u and l indicate upper and lower eyelids, respectively (μm)
$L_{im,PrCj}$: Arc length of eyelid at pre-conjunctival tear-film region. i = u and l indicate upper and lower eyelids, respectively (μm)
P: Applied pressure (Pa)
Pe: Péclet number (Equation C3)
q_{cn}: Volumetric flow rate of water from the cornea ($\mu L/min$)
q_{cj}: Volumetric flow rate of water from the bulbar conjunctiva into the pre-conjunctival tear film ($\mu L/min$)
q_d: Volumetric tear drainage rate. Sum of q_{du} and q_{dl} ($\mu L/min$)
q_{di}: Volumetric tear drainage rate. Drainage through puncta. i = u and l indicate upper and lower puncta, respectively ($\mu L/min$)
q_e: Volumetric tear evaporation rate ($\mu L/min$)
$q_{e,im}$: Volumetric evaporation rate of the upper and lower menisci. i = u and l indicate upper and lower menisci, respectively ($\mu L/min$)
$q_{e,PrCj}$: Volumetric tear evaporation rate for pre-conjunctival tear film ($\mu L/min$)
$q_{e,PrL}$: Volumetric tear evaporation rate for the pre-lens tear film ($\mu L/min$)
q_{lac}: Volumetric aqueous production rate ($q_{lacu}+q_{lacl}$) ($\mu L/min$)
q_{lacl}: Volumetric flow rate of water entering the lower meniscus from the conjunctival sac ($q_{lacl} = 0.2q_{lac}$) ($\mu L/min$)
q_{lacu}: Volumetric flow rate of water entering the upper meniscus from the conjunctival sac ($q_{lacu} = 0.8q_{lac}$) ($\mu L/min$)
q_{lens}: Volumetric water transport rate across the lens ($\mu L/min$)
q_m: Maximum volumetric tear drainage rate ($\mu L/min$)
Q: Volumetric air flow rate (cm^3/s)
R: Ideal gas constant ($J/(mol \times K)$)
R_0: Meniscus radius when drainage ceases (μm)
R_H: Relative humidity
R_{im}: Tear meniscus radius. i = u and l indicate upper and lower menisci, respectively (μm)
s: Laplace variable
S: Obstruction factor
S_{lid}: Lid-margin perimeter (cm)
t: Time (s)
t_{ib}: Interblink period (s)
T: Temperature (K)
T_{95}: Time to deplete 95% of the fluorescein from the PoLTF (s)
u_{lid}: Velocity of upper eyelid (m/s)
$u_{s,j}$: Velocity of j where j = PrCj and PrL indicate bulbar conjunctiva and soft contact lens, respectively (m/s)
v_w: Water superficial velocity and is equivalent to $\widetilde{J}_{w,lens}$ (m/s)
V_{blink}: Tear volume produced by the lacrimal glands during the blink phase (μL)
V_{im}: Meniscus volume. i = u and l indicate upper and lower menisci, respectively (μL)
V_{PoL}: Volume of water in the post-lens tear film (μL)
V_{PrCj}: Volume of water in the pre-conjunctival tear film (μL)
V_{PrL}: Volume of water in the pre-lens tear film (μL)
V_{si}: Conjunctival sac tear volume. i = u and l indicate upper and lower conjunctival sacs, respectively (μL)
V_{total}: Total volume of the tear mixed during a blink phase (μL)
x: Spatial location from the center of the pre-lens tear film to the periphery (cm)
z: Spatial location within the lens from the posterior ($z = 0$) to the anterior of the soft contact lens (μm)
α: Fraction of bulbar conjunctiva that is not covered by the soft contact lens and the eyelids
β: Fraction of post-lens tear film that mixes with the rest of the tear during each blink cycle
γ: Tear surface tension (mN/m)
Δc_{cn}: Salt concentration difference between the post-lens tear film and the corneal epithelium (mol/m^3)
θ: Dimensionless salt concentration
$\overline{\theta}$: Dimensionless Laplace salt concentration (Equation E5)
λ: Distance from the meniscus or the pre-conjunctival tear film to the soft-contact-lens center (cm)
μ_w: Tear viscosity ($mPa \times s$)
Π: Osmotic pressure (Pa)
σ_{cn}: Corneal epithelium reflection coefficient of salt
τ_H: Lens hydrodynamic tortuosity
τ_s: Lens salt tortuosity
τ: Dimensionless time
φ: Polymer volume fraction of soft contact lens
φ_w: Water volume fraction of soft contact lens
X: Dimensionless x
ω_{cn}: Corneal epithelium membrane permeability of salt (m/s)
$< c_{cn} >$: Arithmetic average salt concentration in the corneal epithelium interface (mol/m^3)